

**NASA SUN-EARTH CONNECTIONS THEORY PROGRAM  
CONTRACT NAS5-99188**

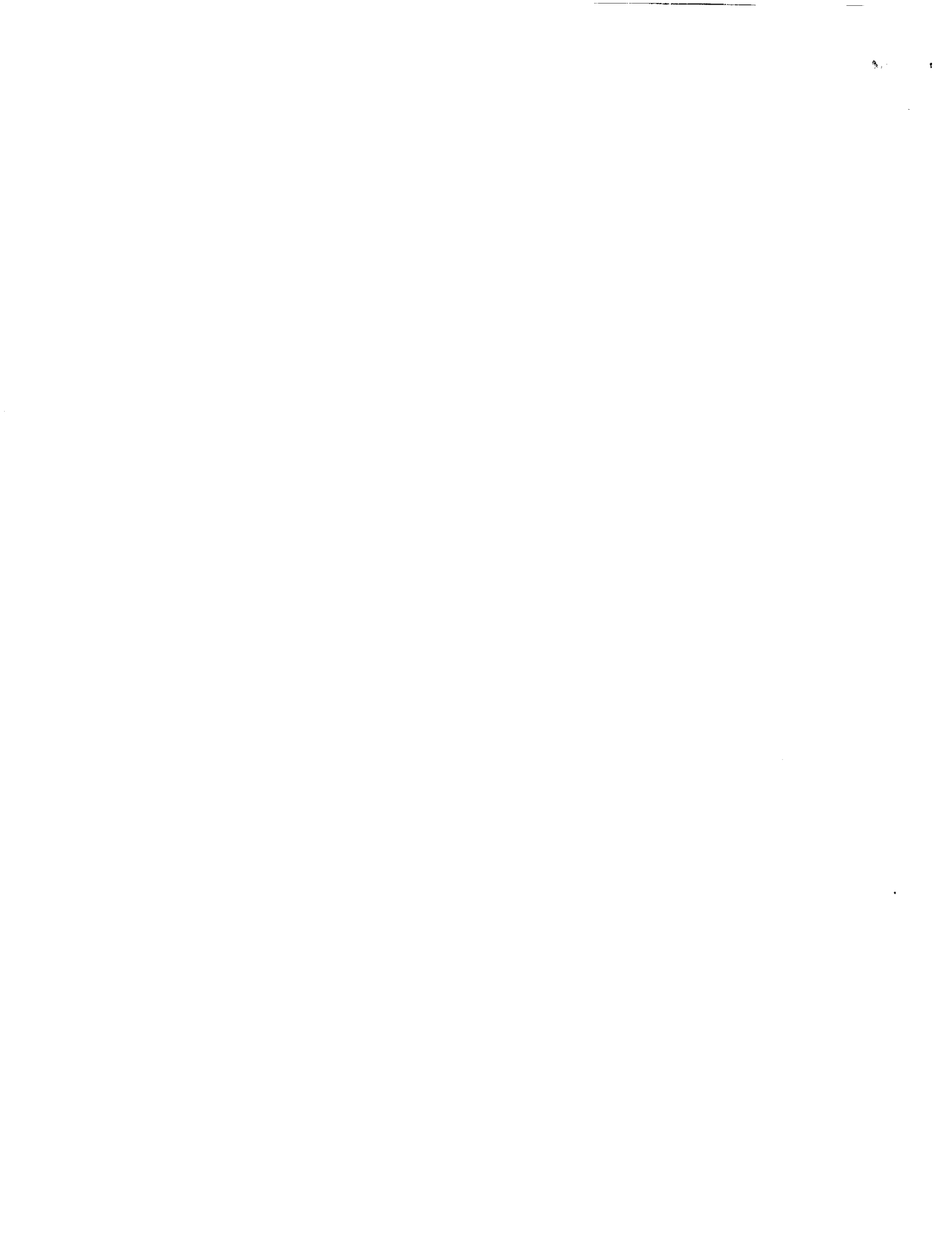
The Structure and Dynamics of the Solar Corona  
and Inner Heliosphere

**FOURTH QUARTER SECOND YEAR PROGRESS REPORT**  
Covering the period May 16, 2001 to August 15, 2001

Submitted by:

Zoran Mikić  
Principal Investigator  
Science Applications International Corporation  
10260 Campus Point Drive  
San Diego, CA 92121

August 15, 2001



## FOURTH QUARTER SECOND YEAR PROGRESS REPORT

This report covers technical progress during the fourth quarter of the second year of NASA Sun-Earth Connections Theory Program (SECTP) contract "The Structure and Dynamics of the Solar Corona and Inner Heliosphere," NAS5-99188, between NASA and Science Applications International Corporation, and covers the period May 16, 2001 to August 15, 2001. Under this contract SAIC and the University of California, Irvine (UCI) have conducted research into theoretical modeling of active regions, the solar corona, and the inner heliosphere, using the MHD model.

### Press Release at the Spring AGU Meeting, Boston, MA, May 30, 2001

Zoran Mikić was invited by the AAS/SPD press officer, Dr. Criag DeForest, to give a presentation at a press conference about the total solar eclipse that was expected in Africa on June 21, 2001. An accompanying press release is contained in Appendix A.

### Presentations at the Spring AGU Meeting, Boston, MA, May 29–June 2, 2001

Our progress during this reporting period is summarized by the following papers that were presented by SAIC staff members at the Spring AGU Meeting, Boston, MA, May 29–June 2, 2001.

#### *Predicting the Structure of the Solar Corona During the 21 June 2001 Total Solar Eclipse*

Z. Mikić, J. A. Linker, R. Lionello, and P. Riley (SAIC, San Diego)

We describe the application of a three-dimensional magnetohydrodynamic (MHD) model to the prediction of the structure of the corona during the total solar eclipse that is expected to occur on 21 June 2001. The calculation uses the observed photospheric radial magnetic field as a boundary condition. This model makes it possible to determine the large-scale structure of the magnetic field in the corona, as well as the distribution of the solar wind velocity, plasma density, and temperature. We will use magnetic fields observed on the solar disk prior to eclipse day to predict what the corona will look like during the eclipse. The estimated coronal density will be used to predict the plane-of-sky polarization brightness prior to the eclipse.

A copy of this presentation appears in Appendix B.

---

#### *Are There Two Classes of Coronal Mass Ejections? A Theoretical Perspective\**

J. A Linker, Z. Mikić, R. Lionello, and P. Riley (SAIC, San Diego)

Coronal mass ejections (CMEs) are generally accepted as the cause of nonrecurrent magnetic storms at Earth. Statistical compilations of CME events have shown that CMEs launched in the corona can have a wide variation in speeds (Hundhausen *et al.*, *JGR* **99**, 6543, 1994). The speed of the CME at Earth and the presence or absence of an interplanetary shockwave is an important component of the geoeffectiveness; therefore, the mechanism(s) by which fast CMEs might be produced are considered to be of particular importance. Recently,

the examination of the acceleration profiles of CMEs has led to the possible classification of CMEs as either constant speed CMEs or constant acceleration (St. Cyr *et al.*, *JGR* **104**, 12493, 1999; Sheeley *et al.*, *JGR* **104**, 24739, 1999). In this talk, we will examine reasons why one might expect CMEs to show two classes of acceleration profiles, and if they do, what the implications are for models of CME initiation. Examples from MHD simulations of CMEs for different initiation mechanisms will be used to illustrate essential points.

\*Research supported by NASA and Boston University's Integrated Space Weather Modeling project (funded by NSF).

A copy of this presentation appears in Appendix C.

---

*Using Global MHD Simulations to Interpret In Situ Observations of CMEs*

P. Riley, J. A. Linker, R. Lionello, Z. Mikić (SAIC, San Diego)  
D. Odstrcil, V. J. Pizzo (SEC, Boulder)  
T. H. Zurbuchen (U. Michigan)  
D. Lario (JHU/APL)

In this study, we combine two MHD models to simulate the initiation, propagation, and dynamic evolution of flux-rope-like CMEs through the corona and out to 1 AU. The coronal model encompasses the region of the solar corona from  $1R_s$  to  $20R_s$ , while the heliospheric model encompasses  $20R_s$  to 1 AU. The CME initiated in the corona propagates smoothly across the outer boundary of the coronal solution and through the inner boundary of the heliospheric solution. The model solutions show a rich complexity, which, given the relative simplicity and idealization of the input conditions, bear a strong resemblance to many observed events, and we use the simulation results to infer the global structure of some of these observations. In particular, we highlight an event that was observed by both Ulysses and ACE in February/March, 1999. At this time, Ulysses was located at  $\sim 5$  AU and  $22^\circ$ S heliographic latitude; thus the two spacecraft were separated significantly both in heliocentric distance and latitude. We also use these simulations to separate dynamical effects from force-free models of flux ropes in the solar wind.

A copy of this presentation appears in Appendix D.

---

*Modeling of Transequatorial Loops with MH4D*

R. Lionello and D. Schnack (SAIC, San Diego)

MH4D (Magnetohydrodynamics on a TETRAhedral Domain) is a new algorithm to perform magnetohydrodynamic (MHD) simulations of the active regions of the Sun, including the large scale coronal structure that surround them. MH4D is a massively-parallel, device-independent numerical code for the advancement of the resistive and viscous MHD equations on an unstructured grid of tetrahedra. The use of an unstructured grid allows us to increase the resolution in the regions of physical interest. A variational formulation of the differential operators ensures accuracy and the preservation of the analytical properties of the operators

( $\nabla \cdot \mathbf{B} = 0$ , self-adjointness of the resistive and viscous operators). The combined semi-implicit treatment of the waves and implicit formulation of the diffusive operators can accommodate the wide range of time scales present in the solar corona. The capability of mesh refinement and coarsening is also included. A preliminary result is presented: a simulation of transequatorial loops that include fine details of two interconnected active regions.

A copy of this presentation appears in Appendix E.

## **APPENDIX A**

Press Release at the Spring AGU Meeting  
Boston, MA, May 30, 2001  
Presented by Zoran Mikić

## PREDICTING THE STRUCTURE OF THE SOLAR CORONA DURING THE 21 JUNE 2001 TOTAL SOLAR ECLIPSE

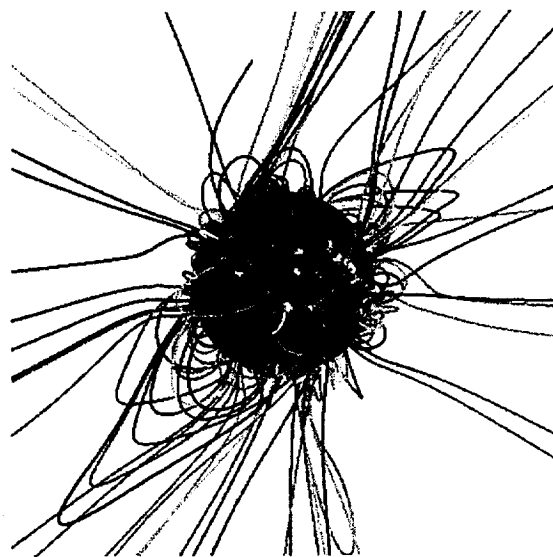
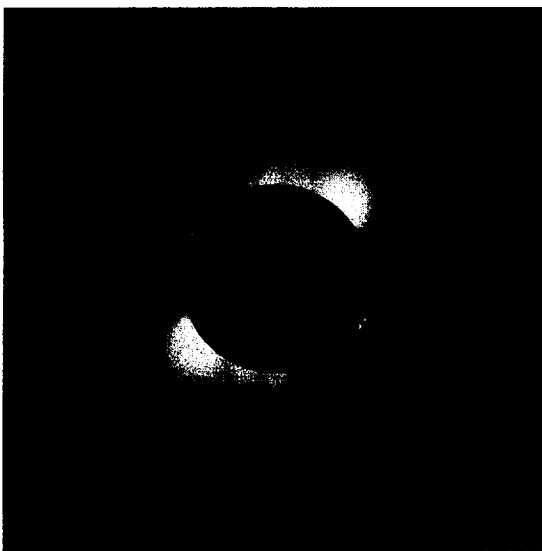
Total solar eclipses offer an excellent opportunity to observe the solar corona. During a total solar eclipse the moon blocks the bright light from the solar disk, allowing the faint light scattered by the solar corona, which is more than a million times fainter than the photosphere, to become visible. During totality the structures that characterize the white-light corona become apparent, including prominences, helmet streamers, polar plumes, and coronal holes. Observers who witness a total solar eclipse invariably report that it is a beautiful sight to behold.

On 21 June, 2001 a total eclipse of the Sun will be visible in the southern hemisphere, beginning in the South Atlantic, crossing southern Africa and Madagascar, and terminating in the Indian Ocean. Drs. Zoran Mikić, Jon Linker, Pete Riley, and Roberto Lionello, of Science Applications International Corporation (SAIC) in San Diego, California, have developed a theoretical model to predict what the solar corona will look like during forthcoming total solar eclipses. Their model has been used to predict the shape of the corona during the eclipse that is expected to occur on 21 June.

The model is based on the three-dimensional magnetohydrodynamic (MHD) equations that describe the interaction of the solar wind with coronal magnetic fields. The group's results, which have been financially supported by the National Aeronautics and Space Administration (NASA) and the National Science Foundation (NSF), are being presented by Dr. Mikić at the American Geophysical Union meeting in Boston.

The calculation relies on Earth-based measurements of the magnetic field in the solar photosphere to infer the structure of the solar corona. The measurements are taken at the National Solar Observatory at Kitt Peak. "It is remarkable that measurements of the magnetic field in the photosphere can tell us so much about the corona," says Dr. Mikić. "The simulations already have a strong resemblance to coronal images. In the future, the agreement will only improve as we refine the physics in our model and as we utilize ever-faster computers. We will be able to study even finer details in the corona." The researchers use supercomputers at the San Diego Supercomputer Center (part of NSF's National Partnership for Advanced Computing Infrastructure) and the Department of Energy's National Energy Research Supercomputer Center to solve the equations. The output from the model is used to predict the brightness of the corona.

So far, this model has been applied to five eclipses (see <http://haven.saic.com>). This kind of modeling helps us to understand the structure of the solar corona, especially the location of helmet streamers and coronal holes, and the nature of the fast and slow solar wind, and provides a rudimentary test of predictive capability. Eclipses offer an opportunity to test such models, and to understand the influence of the Sun on the Earth.



Predicted polarization brightness (pB) for the 21 June, 2001 eclipse, together with traces of the magnetic field lines, at 13:10 UT (corresponding to totality in Lusaka, Zambia). The pB signal is produced by white light scattered off electrons in the coronal plasma. This is the view of the Sun that would be seen by an observer on Earth with a camera aligned so that vertical is toward the Earth's north pole.

## **APPENDIX B**

“Predicting the Structure of the Solar Corona During the 21 June 2001 Total Solar Eclipse”

Z. Mikić, J. A. Linker, R. Lionello, and P. Riley

Presented at the Spring AGU Meeting

Boston, MA, May 29–June 2, 2001

# PREDICTING THE STRUCTURE OF THE SOLAR CORONA DURING THE 21 JUNE 2001 TOTAL SOLAR ECLIPSE\*

ZORAN MIKIĆ

JOHN A. LINKER

PETE RILEY

ROBERTO LIONELLO

SCIENCE APPLICATIONS INTL. CORP.  
SAN DIEGO

Presented at the Meeting of the  
American Geophysical Union,  
Boston, May 29–June 2, 2001

\*Supported by NASA and NSF

## INTRODUCTION

- The solar magnetic field plays a key role in determining coronal
  - The principal input to MHD models is the observed solar magnetic field
  - 3D MHD models can be used to compare with eclipse and coronagraph images, SOHO images (LASCO, EIT), Ulysses and WIND spacecraft data, and interplanetary scintillation (IPS) measurements
  - MHD computations can tell us about the structure of the corona
  - Eclipses can help us to verify the accuracy of the models
- **21 June, 2001 total solar eclipse:** visible in the southern hemisphere, (South Atlantic, southern Africa, Madagascar, and Indian Ocean)
  - Totality in Lusaka, Zambia is at 13:10UT

## NON-LINEAR EQUATIONS

### THE POLYTROPIC MODEL

- Neglect thermal conduction, coronal heating, radiation loss, and Alfvén waves (set  $p_w = 0$  and  $S = 0$ )
- Simulate these effects (crudely) by setting  $\gamma = 1.05$  (Parker 1963)
- A possible extension is to have  $\gamma = \gamma(r)$ , with  $\gamma$  increasing far from the Sun
- We have used this model extensively in 3D computations of the structure and dynamics (e.g., CMEs) of the solar corona
- The corona is modeled reasonably well, but the properties of the interplanetary solar wind are not accurate (speed, density, temperature)
- An improved model (with more accurate energy transport) is being developed

$$\nabla \times \mathbf{B} = \frac{4\pi}{c} \mathbf{J}$$

$$\nabla \cdot \mathbf{B} = -\frac{1}{c} \frac{\partial \mathbf{B}}{\partial t}$$

$$\mathbf{E} + \frac{1}{c} \mathbf{v} \times \mathbf{B} = n \mathbf{J}$$

$$\frac{\partial \rho}{\partial t} + \nabla \cdot (\rho \mathbf{v}) = 0$$

$$\begin{aligned} \rho \left( \frac{\partial \mathbf{v}}{\partial t} + \mathbf{v} \cdot \nabla \mathbf{v} \right) &= \frac{1}{c} \mathbf{J} \times \mathbf{B} - \nabla p - \nabla p_w \\ &\quad + \rho \mathbf{g} + \nabla \cdot (\nu \rho \nabla \mathbf{v}) \\ \frac{\partial p}{\partial t} + \nabla \cdot (p \mathbf{v}) &= (\gamma - 1)(-\rho \nabla \cdot \mathbf{v} + S) \end{aligned}$$

## MHD EQUATIONS (POLYTROPIC MODEL)

$$\nabla \times \mathbf{B} = \frac{4\pi}{c} \mathbf{J}$$

$$\nabla \times \mathbf{E} = -\frac{1}{c} \frac{\partial \mathbf{B}}{\partial t}$$

$$\begin{aligned} \mathbf{E} + \frac{1}{c} \mathbf{v} \times \mathbf{B} &= n \mathbf{J} \\ \frac{\partial \rho}{\partial t} + \nabla \cdot (\rho \mathbf{v}) &= 0 \\ \rho \left( \frac{\partial \mathbf{v}}{\partial t} + \mathbf{v} \cdot \nabla \mathbf{v} \right) &= \frac{1}{c} \mathbf{J} \times \mathbf{B} - \nabla p \\ &\quad + \rho \mathbf{g} + \nabla \cdot (\nu \rho \nabla \mathbf{v}) \\ \frac{\partial p}{\partial t} + \nabla \cdot (p \mathbf{v}) &= -(\gamma - 1)p \nabla \cdot \mathbf{v} \\ \gamma &= 1.05 \end{aligned}$$

## FINDING MHD SOLUTIONS

- Use line-of-sight magnetograms to deduce  $B_r$  from  $B_{\text{los}}$  at  $r = R_o$  (e.g., Kitt Peak Solar Observatory and Wilcox Solar Observatory synoptic maps)
- Calculate a potential field matching  $B_r$  at  $r = R_o$
- Specify  $T$  and  $\rho$  on the solar surface  $r = R_o$  (e.g., uniform  $T_o$  and  $\rho_o$ )
- Set up  $p$ ,  $\rho$ , and  $\mathbf{v}$  from a spherically symmetric solar wind (1D Parker solution)
- Integrate 3D MHD equations in time until steady state is reached
  - This gives the structure of the coronal magnetic field  $\mathbf{B}$  (as well as  $p$ ,  $\rho$ ,  $\mathbf{v}$ ,  $T$ )
  - Compare with observations

## POLARIZATION BRIGHTNESS

- Light scattered off the coronal electrons is observed in coronagraphs

$$pB(\mathbf{x}) = K \int_{\text{los}} n_e(\mathbf{x} - \mathbf{x}') C(r') dl'$$

- $C(r)$  is a scattering function (e.g., Billings 1966)
- To produce a plane-of-sky image, we apply a (radial) filter to  $pB$  ("vignetting function") and we simulate the effect of an occulting disk

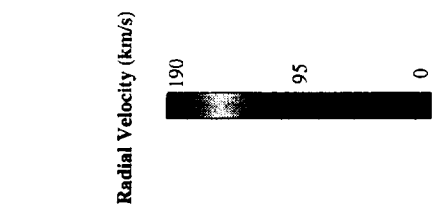
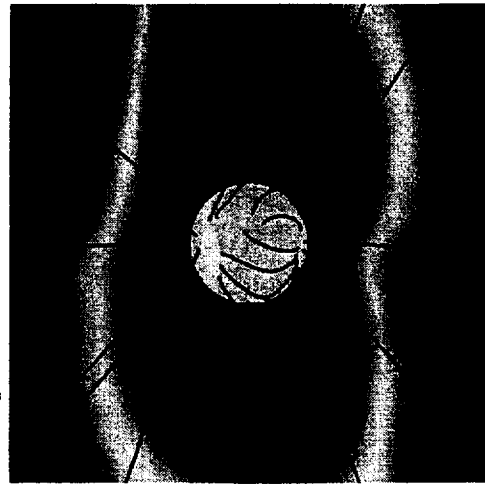
## "CANONICAL" HELMET STREAMER

- Idealized helmet streamer configuration
- Start with 2D (axisymmetric) dipole field (Pneuman & Kopp 1971)
- Closed-field region with a static ( $\mathbf{v} = 0$ ) dense plasma, surrounded by an open-field region with solar wind streaming along the field lines
- A current sheet surrounds the helmet, and an equatorial current-sheet separates fields of opposite polarity

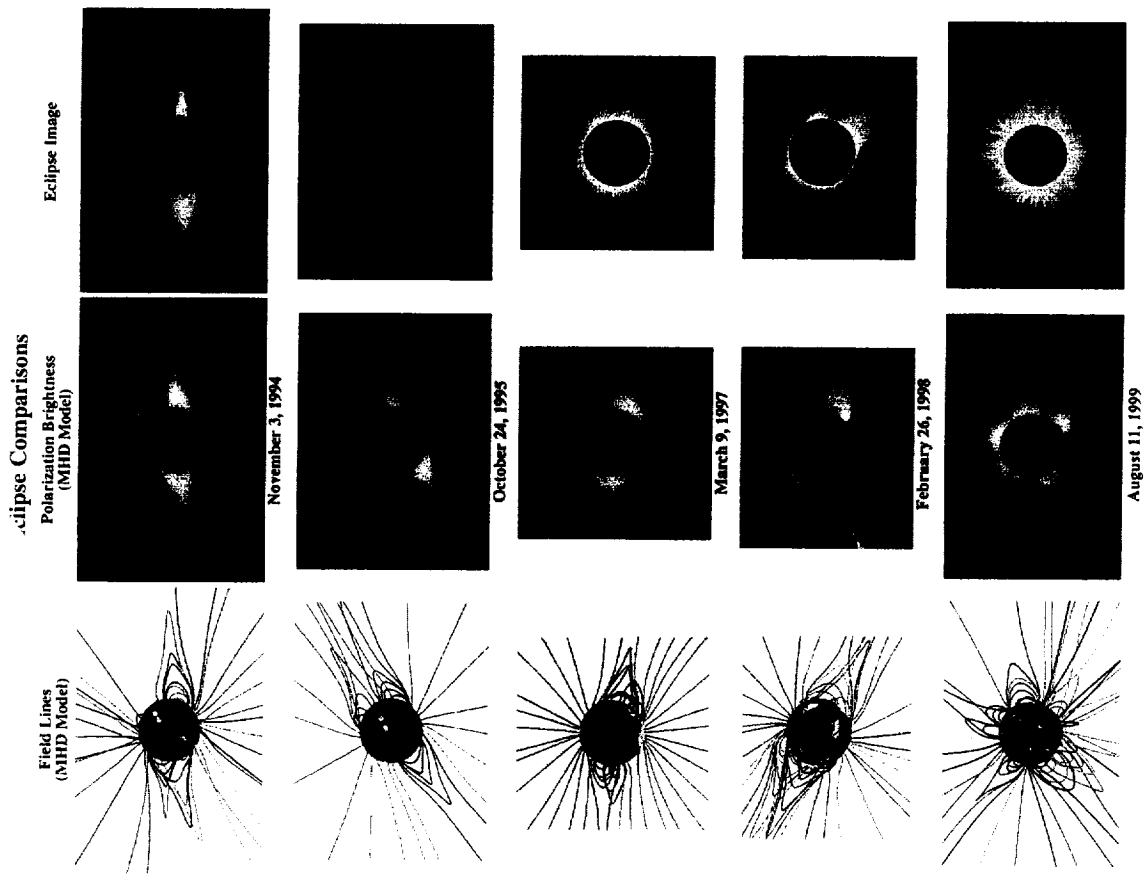
Whole Sun Month  
Aug. 10 - Sep. 8, 1996

## COMPARISON WITH ECLIPSE AND CORONAGRAPH OBSERVATIONS

Radial Velocity  
Open and Closed Field Lines

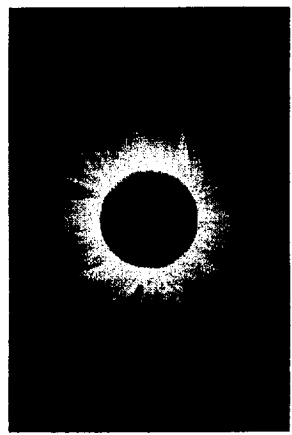


- **November 3, 1994 eclipse (Chile):**  
Compare with eclipse image (HAO) and Mauna Loa coronagraph data
- **October 24, 1995 eclipse (Vietnam):**  
We predicted the coronal structure on Oct. 5, 1995  
Compare with eclipse image (S. Koutchmy)
- **March 9, 1997 eclipse (Russia, China, & Mongolia):**  
We predicted the coronal structure on Mar. 3, 1997  
Compare with eclipse image (E. Hiei)
- **February 26, 1998 eclipse (Caribbean):**  
We predicted the coronal structure on Feb. 13, 1998  
Compare with eclipse image (HAO)

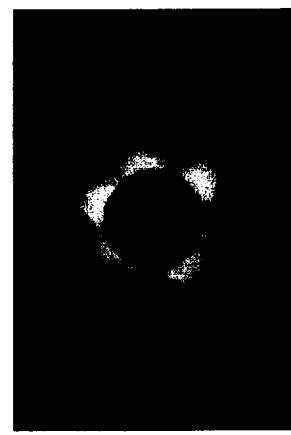


- **August 11, 1999 eclipse (Central Europe, Turkey, Iran):**  
We predicted the coronal structure on July 28, 1999  
Compare with eclipse image (Espenak)

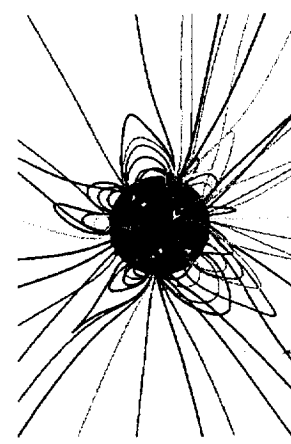
## Comparison of a 3D MHD Coronal Prediction with an Image of the 11 August 1999 Total Solar Eclipse



Fred Espenak's Composite Image (Turkey)



Predicted Polarization Brightness (MHD Model)



Predicted Magnetic Field Lines (MHD Model)

## Evolution of the Photospheric Magnetic Field Leading up to the August 11, 1999 Total Solar Eclipse (Courtesy of Kitt Peak Solar Observatory)

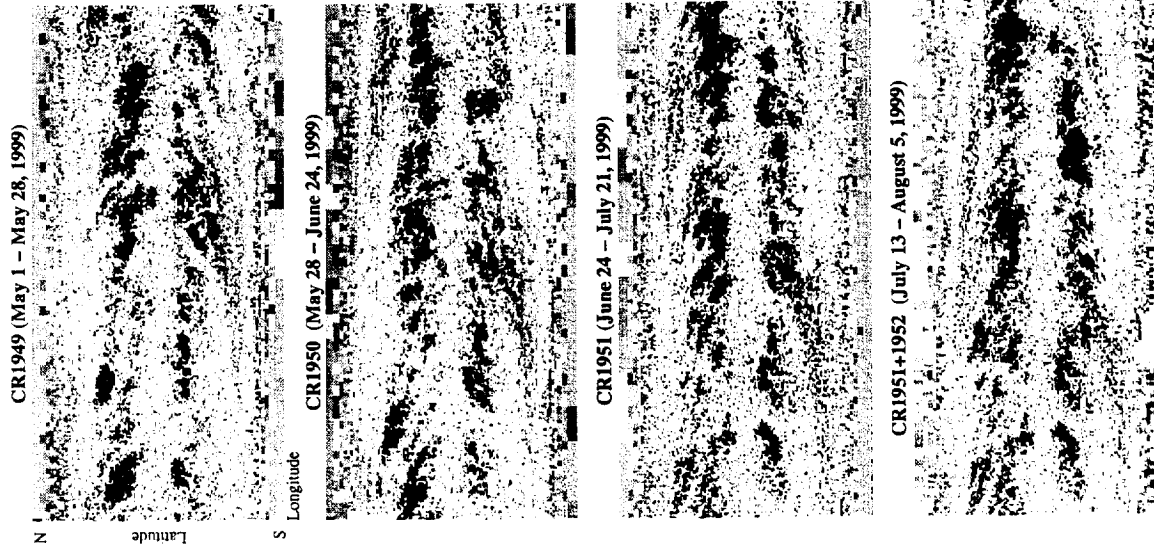
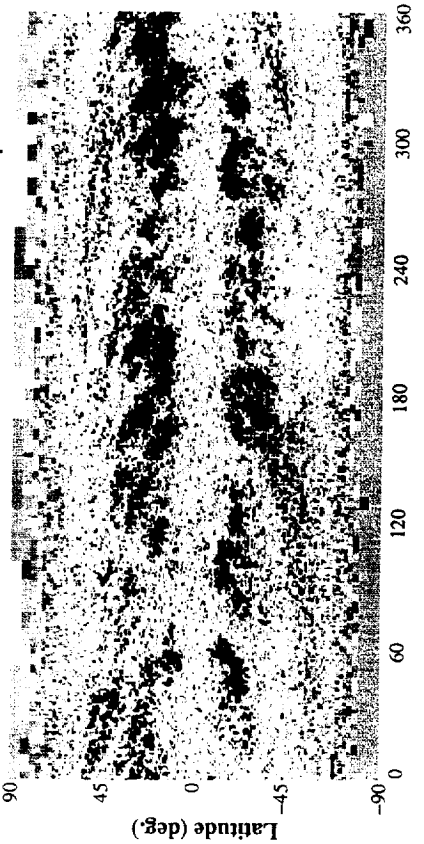


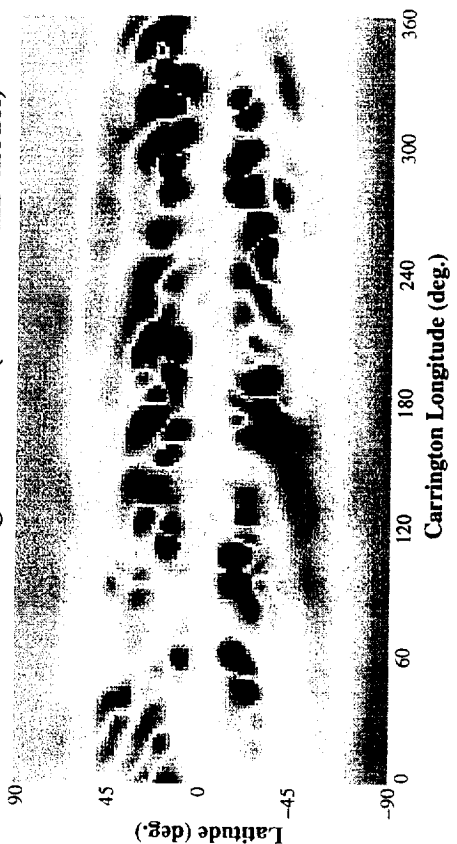
Figure 1. Comparison between a composite image created from photographs taken by Fred Espenak in Lake Hazar, Turkey (top) with the predicted polarization brightness of the simulated solar corona from our 3D MHD model (middle). The projected magnetic field lines from the model are also shown (bottom). Terrestrial (geocentric) north is vertically upward. The eclipse image is copyrighted 1999 by Fred Espenak.

## August 11, 1999 Total Solar Eclipse

Kitt Peak Synoptic Chart (CR1951),  $B_r$



Smoothed Magnetic Field (used in MHD model)



## JUNE 21, 2001 SOLAR ECLIPSE PREDICTION

- Started a high-resolution simulation on May 19, 2001 using magnetic field data from a Kitt Peak Solar Observatory synoptic map of CR1975 (April 9-May 6, 2001).
- Low-resolution case:  $61 \times 71 \times 64$  ( $r, \theta, \phi$ ) mesh points (~7 CPU hrs on the Cray-T90)
- High-resolution case:  $111 \times 101 \times 128$  ( $r, \theta, \phi$ ) mesh points (~90 CPU hrs on the Cray-T90)
- This calculation will be updated in the next few weeks with more recent magnetic field data
- The code runs on PCs and Cray computers. It is also being developed to run on massively parallel machines using MPI (e.g., Cray T3E, Beowulf, IBM SP3)

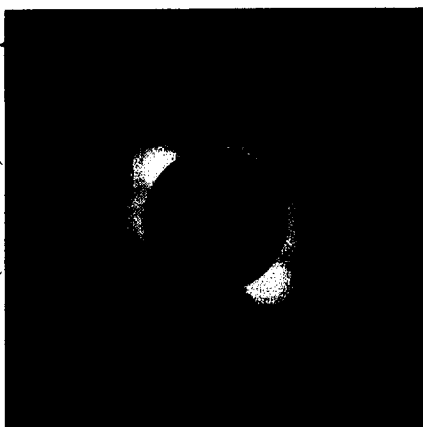
- See:

<http://haven.saic.com/corona/modeling.html>

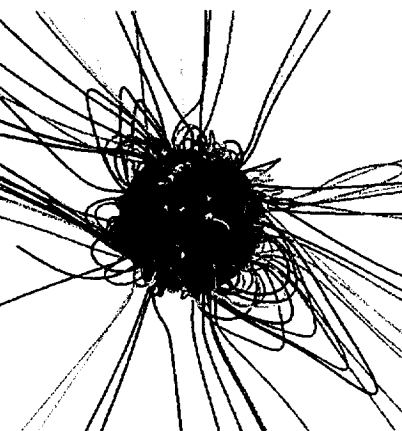
## Prediction of the Structure of the Solar Corona for the 21 June 2001 Eclipse

### Predicted Polarization Brightness

Geocentric (terrestrial) north is up



**Magnetic Field Lines**  
 $B_r$  contoured on the surface



Predicted on May 19, 2001 using magnetic field data from Kitt Peak Solar Observatory for Carrington rotation 1975 (April 9 - May 6, 2001).

<http://haven.sacit.com>

Tuesday May 29 2001

June 21: Total Eclipse

Page 1

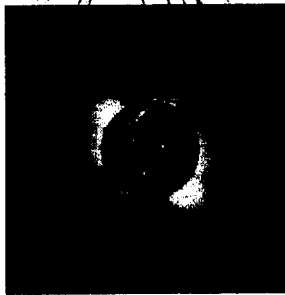
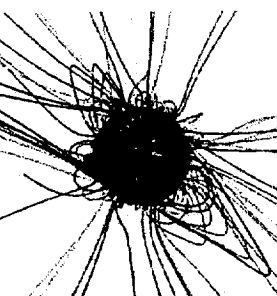
## Predicting the Structure of the Solar Corona During the 21 June, 2001 Total Solar Eclipse

On Thursday, 21 June, 2001, a total eclipse of the Sun will be visible from within a narrow corridor crossing the Southern Hemisphere, beginning in the South Atlantic, crossing southern Africa and Madagascar, and terminating in the Indian Ocean. A partial eclipse can be seen throughout Eastern South America and mid-south Africa. To see a detailed description of the eclipse, please visit [Eclipse.2001.TotalEclipse.info](http://eclipse.2001.TotalEclipse.info).

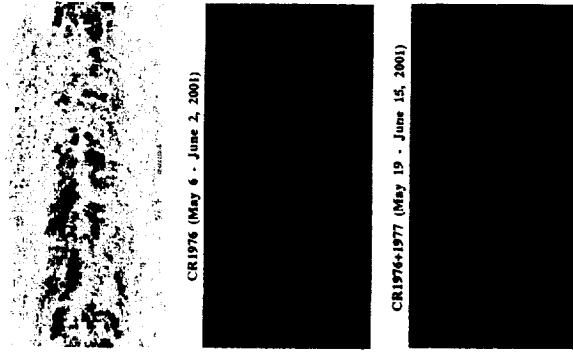
On 19 May, 2001, we started an MHD simulation of the solar corona in preparation for our prediction of what the solar corona will look like during this eclipse. We used photospheric magnetic field data from Carrington rotation 1975 (corresponding to the dates April 9 - May 6, 2001) from the National Solar Observatory at Kitt Peak. We will refine this prediction in the next few weeks using more recent photospheric magnetic field data. After the eclipse, we will compare between our prediction and images taken on the day of the eclipse.



The figure on the left shows the predicted polarization brightness ( $B_{\parallel}$ ) in the solar corona for the eclipse expected on 21 June, 2001 at 13:11 LT (corresponding to 16:11 in London, UK). The state of the solar corona has been predicted using a 1D magnetohydrodynamic (MHD) simulation. The plasma density is produced by what is known as a "local" model of electrons, the ion and wave densities have been read off of a model of the solar wind. The field lines are radial, except near the Sun. Vertical (top) is a residual (geocentric) vector. This is the view of the Sun that would be observed on Earth with a camera aligned so that its optical axis is pointed at the Sun's north pole. To view this image in a coordinate system aligned with solar north, click [here](#). Click the image to see it in more detail.



Predicted polarization brightness (top left) together with traces of the magnetic field lines in the solar corona (top right) for the eclipse expected on 21 June, 2001 at 13:10 LT (with terrestrial north up). The Sun's surface shows color contours of the radial component of the measured photospheric magnetic field from Kitt Peak National Solar Observatory, showing the location of active regions (strong magnetic fields). Click the images for higher resolution pictures. To view these images in a coordinate system aligned with solar north, click [here](#).



the photospheric magnetic field maps we use for our calculations are built up from visual light observations of the Sun during a solar rotation. These maps give a rough approximation of the Sun's magnetic flux if the large-scale flux is not changing much over a rotation. Previously, we have employed coronal models for two eclipses—November 3, 1984 for the beginning of the solar cycle (November 3, 1984) and March 9, 1992, one solar cycle later (October 24, 1992 and March 9, 1992)—one solar cycle during the early rising phase of solar cycle 23 (February 26, 1992), and one eclipse occurring at the peak of solar maximum (August 11, 1992). The photospheric magnetic field is evolving more rapidly, making a synoptic magnetic field data a less reliable approximation to the true state of the photospheric magnetic field. A less systematic use of coronal models requires high resolution runs (requiring approximately 500,000 grid points in our calculation).

These figures show the photospheric magnetic field maps for three Carrington rotations, CR1976, CR1977, and CR1978, as measured by the National Solar Observatory Kitt Peak. The maps show the measured photospheric magnetic field as a function of Carrington longitude (horizontal axis) and Carrington latitude (vertical axis). Red shows northward directed magnetic flux, and blue shows southward directed flux. The red and blue colors indicate the direction of the magnetic field. These maps are considerably more complex than maps obtained at minimum.

15

We have made a movie of the polarization brightness from our MHD simulation of the solar corona during Carrington rotation 1975 (April 9 - May 6, 2001). This illustrates visually how rapidly the solar coronal changes as a result of solar rotation during the maximum phase of the solar cycle. You can get an MPEG version

卷之三

- Other web resources for the eclipse:
  - [Edu-Eclipse 2001 Total Solar Eclipse](#): A great resource for the eclipse, including lots of information and links to other sites.

卷之三

## **APPENDIX C**

“Are There Two Classes of Coronal Mass Ejections? A Theoretical Perspective”

J. A Linker, Z. Mikić, R. Lionello, and P. Riley

Presented at the Spring AGU Meeting

Boston, MA, May 29–June 2, 2001

# ARE THERE TWO CLASSES OF CORONAL MASS EJECTIONS? A THEORETICAL PERSPECTIVE\*

## INTRODUCTION

- Despite many years of study, the origin evolution and of coronal mass ejections (CMEs) is poorly understood.
- What are the underlying physical differences between "fast" and "slow" CMEs?  $\Rightarrow$  Important for Space Weather
- Recently, it has been demonstrated that many CMEs observed with the LASCO coronagraph fall roughly into two classes (Sheeley et al. 1999):
  - (1) CMEs that accelerate up to an asymptotic speed;
  - (2) CMEs that travel at constant speed or decelerate

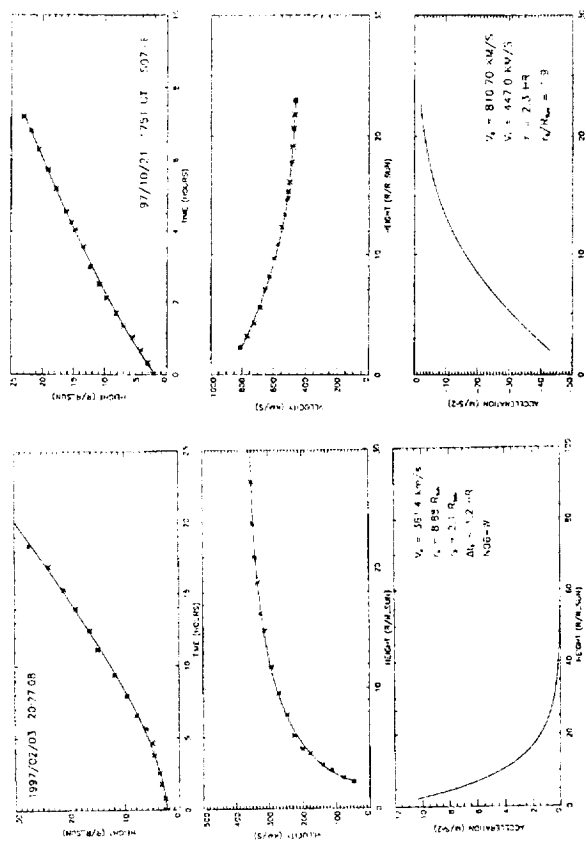
JON A. LINKER  
ZORAN MIKIC  
ROBERTO LIONELLO  
PETE RILEY

*Science Applications International Corporation*

\*Research Supported by NASA and NSF (through Boston University's Integrated Space Weather Modeling Project). Computations performed at NPACI/SDSC.

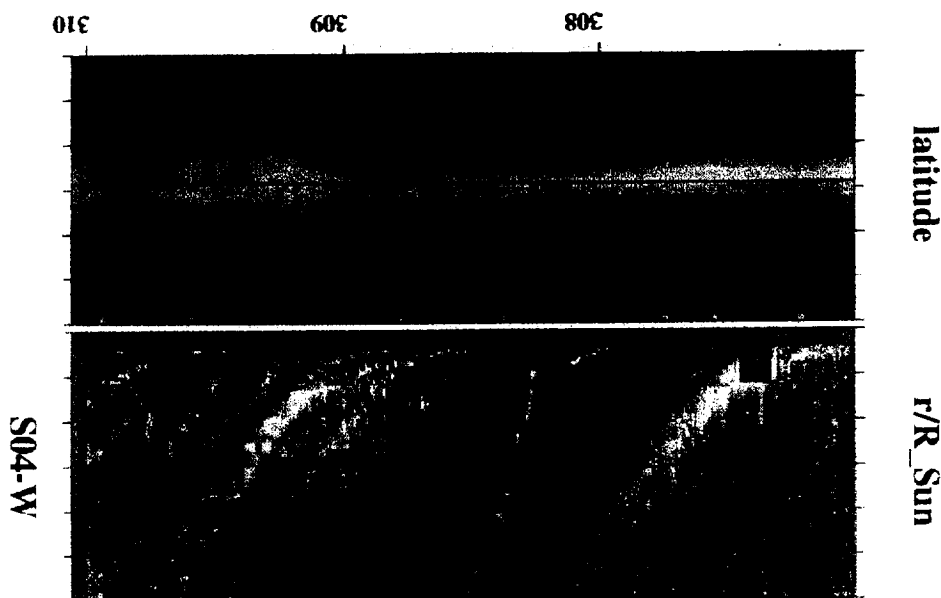
From Sheeley et al., 1999

Decelerating Ejecta



Sheeley et al., 1999

Day of Year



Time Height Plot (LASCO DATA)

## My “ASSIGNMENT:”

“The modelers should address the question of whether there is any theoretical reason why an accelerating CME requires a different expulsion mechanism or environment than a CME that starts out fast and then decelerates.

They should ask themselves whether they can produce the different speed profiles just by varying the source region....

Of course they should also suggest other reasons they can think of that might result in the different speed profiles.”

## QUESTIONS

- Does the division of CMEs into “accelerating” and “constant speed” imply more than one mechanism for CMEs initiation? Does it imply only one mechanism?
- Can we use this classification to help us to understand CME initiation or constrain the possible mechanisms?

## Mechanisms for Solar Activity

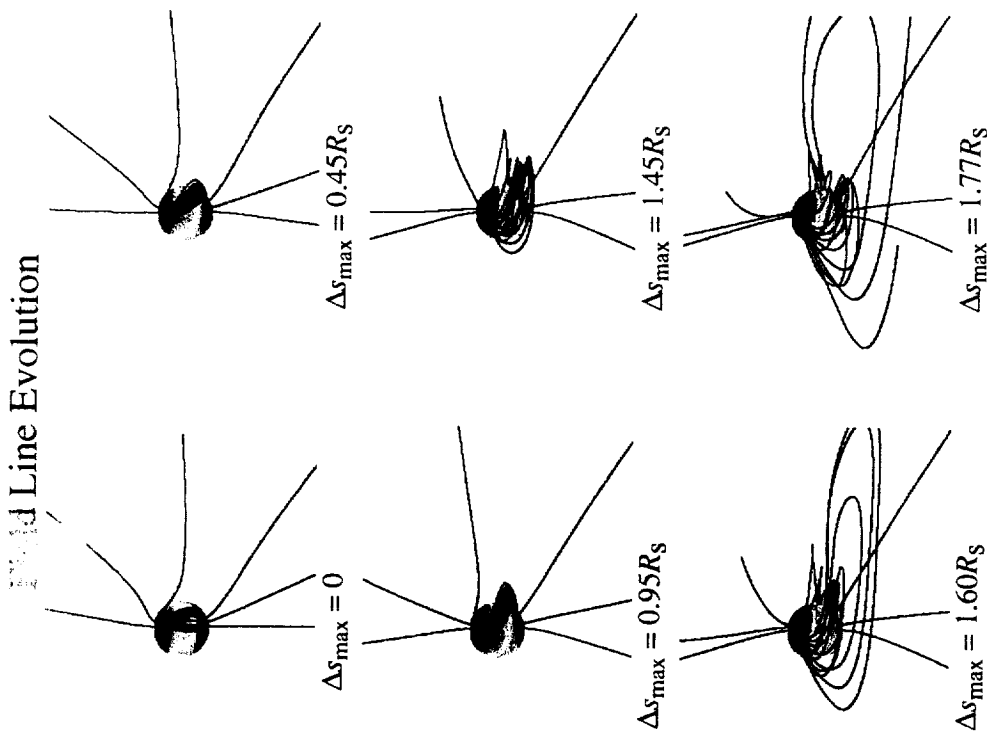
- CMEs, flares, and prominence eruptions require significant amounts of energy ( $\sim 10^{32}$  ergs)
- Most theories assume that energy is released from the coronal magnetic field (see next talk for an opposing view)
- There are many observations of nonpotential magnetic field structures in the corona harboring significant amounts of magnetic energy
- What causes this energy to be released?
  - Many candidate mechanisms
- What sort of time-height profiles of ejecta are implied by different mechanisms? Today we consider two:
  - (1) Shearing of the photospheric magnetic field
  - (2) Magnetic flux cancellation

## ERUPTION BY PHOTOSPHERIC SHEARING FLOWS

- Previously, we showed that photospheric shear leads to the eruption of magnetic field arcades and helmet streamers if the photospheric shear exceeds a threshold (Mikic & Linker 1994, Linker & Mikic 1995)
- Start from a helmet streamer configuration
- Introduce flows (typically 0.5-5 km/s) at the photosphere that twist or shear the magnetic field and energize the configuration.
- When the magnetic shear crosses a threshold, eruption occurs. Eruption threshold does not depend on how fast the shear is introduced.
- Eruption is related to *Magnetic Nonequilibrium* – the appearance of a discontinuity in force-free equilibrium configurations

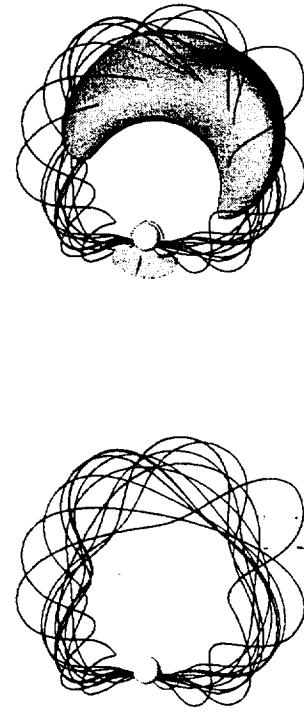
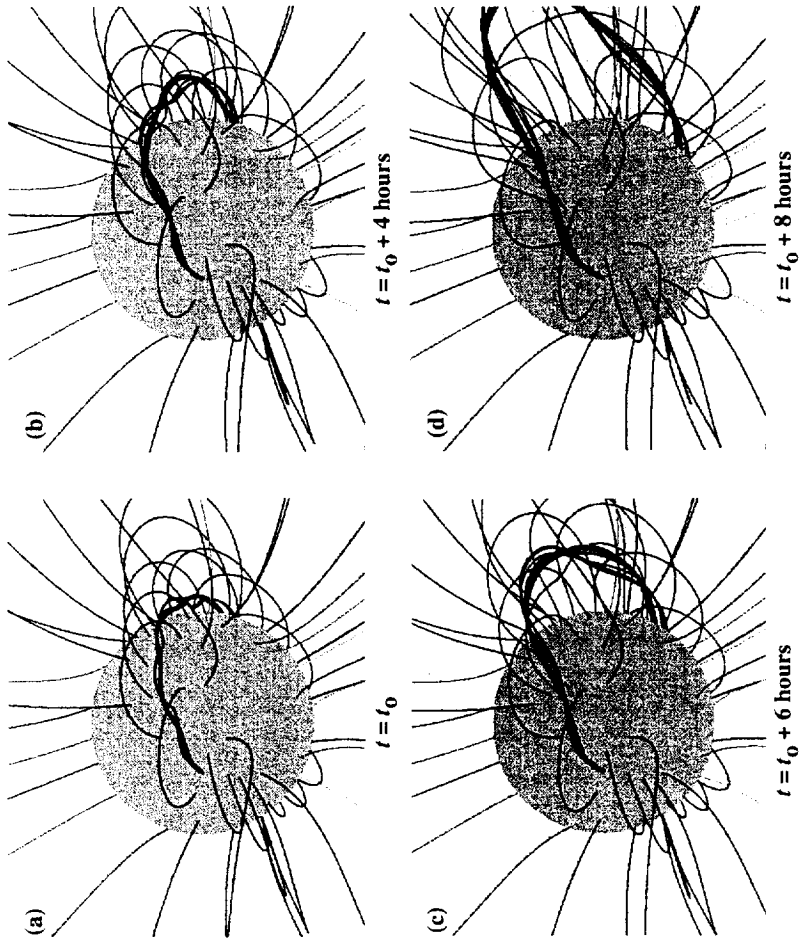
## ERUPTION BY FLUX CANCELLATION

- We have found that reduction of magnetic flux near the neutral line of a sheared or twisted magnetic configuration (i.e., flux cancellation) can lead to the formation of stable flux rope configurations (Amari et al., 1999, 2000; Linker et al., 2001)
- The flux ropes are capable of supporting prominence material in the corona
- When the flux cancellation crosses a threshold, the entire configuration erupts. In the case of a helmet streamer configuration, a CME is ejected into the simulated solar wind.
- The eruption is more energetic than eruptions triggered by photospheric shearing flows.



**Eruption of a 3D Helmet Streamer triggered Shearing Flows**

## Eruption of a 3D Flux Rope



## CONSIDER 5 MODEL PROBLEMS:

- Vary mechanism: Shearing and Flux cancellation
- Vary initial corona: Base temperature  $1.4 \times 10^6$  K or  $1.8 \times 10^6$  K (solar wind speeds of 250 km/s or 350 km/s at  $20R_s$ )
- Performed one flux cancellation simulation with broader shear distribution

## MHD EQUATIONS

$$\nabla \times \mathbf{B} = \frac{4\pi}{c} \mathbf{J}$$

$$\nabla \times \mathbf{E} = -\frac{1}{c} \frac{\partial \mathbf{B}}{\partial t}$$

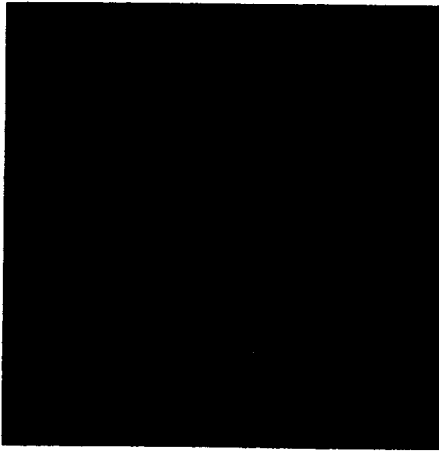
$$\mathbf{E} + \frac{1}{c} \mathbf{v} \times \mathbf{B} = \eta \mathbf{J}$$

$$\frac{\partial \rho}{\partial t} + \nabla \cdot (\rho \mathbf{v}) = 0$$

$$\begin{aligned} \rho \left( \frac{\partial \mathbf{v}}{\partial t} + \mathbf{v} \cdot \nabla \mathbf{v} \right) &= \frac{1}{c} \mathbf{J} \times \mathbf{B} - \nabla p + \rho \mathbf{g} \\ &\quad + \nabla \cdot (\nu \rho \nabla \mathbf{v}) \\ \frac{\partial p}{\partial t} + \nabla \cdot (p \mathbf{v}) &= (\gamma - 1)(-\rho \nabla \cdot \mathbf{v} + S) \end{aligned}$$

## Helmet Streamer Configuration for CME Studies

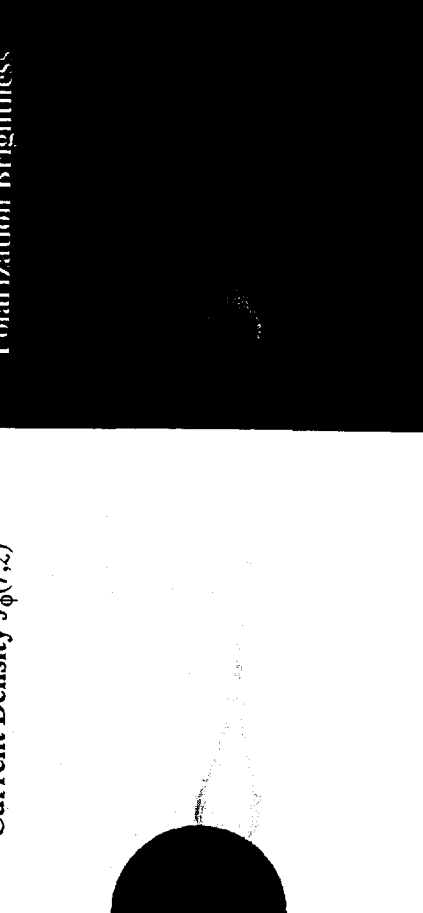
Flux  $\Psi(r,z)$



Initial Potential Field

Relaxed Helmet Streamer

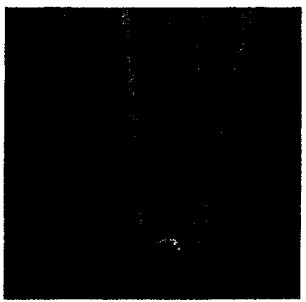
Polarization Brightness



Relaxed Helmet Streamer

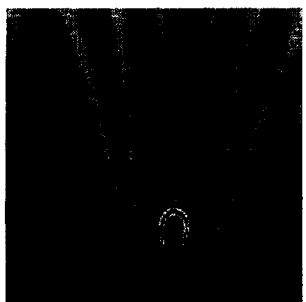
## Eruption of a Helmet Streamer By Emerging Flux

Flux  $\Psi(r,z)$



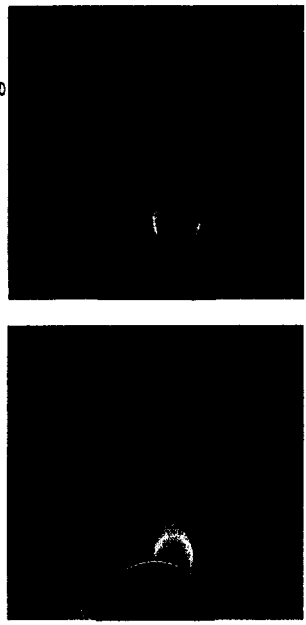
7.5% emerged flux  
 $t = t_0 + 10$  hours

Flux  $\Psi(r,z)$



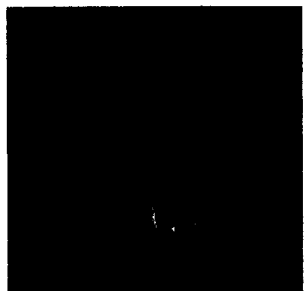
10.5% emerged flux  
 $t = t_0 + 14$  hours

Polarization Brightness



Unsheared streamer  
 $t = t_0$

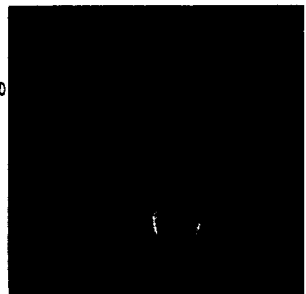
Polarization Brightness



4.5% emerged flux  
 $t = t_0 + 6$  hours

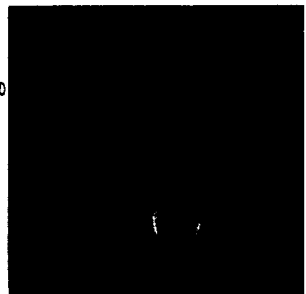
## Eruption of a Helmet Streamer By Emerging Flux

Sheared streamer  
 $t = t_0$



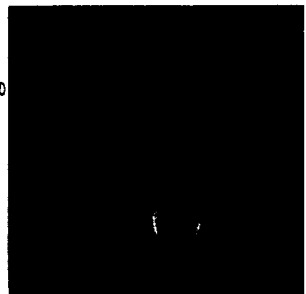
Sheared streamer  
 $t = t_0$

Sheared streamer  
 $t = t_0 + 6$  hours



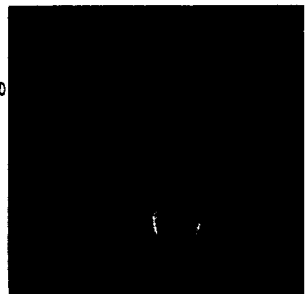
4.5% emerged flux  
 $t = t_0 + 6$  hours

Sheared streamer  
 $t = t_0 + 10$  hours



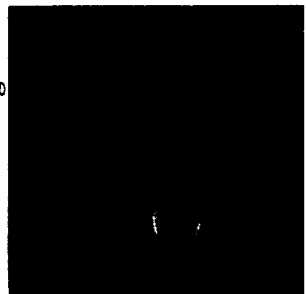
7.5% emerged flux  
 $t = t_0 + 10$  hours

Sheared streamer  
 $t = t_0 + 14$  hours



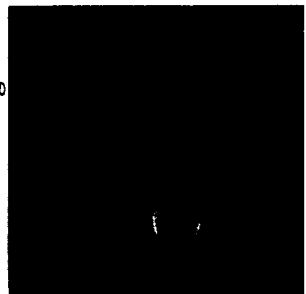
10.5% emerged flux  
 $t = t_0 + 14$  hours

Sheared streamer  
 $t = t_0 + 16$  hours



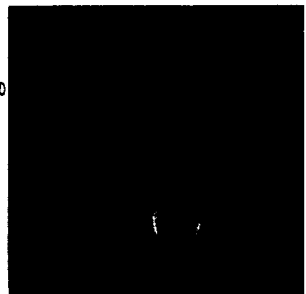
12% emerged flux  
 $t = t_0 + 16$  hours

Sheared streamer  
 $t = t_0 + 20$  hours

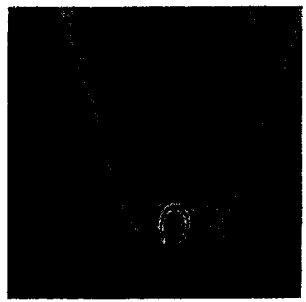


15% emerged flux  
 $t = t_0 + 20$  hours

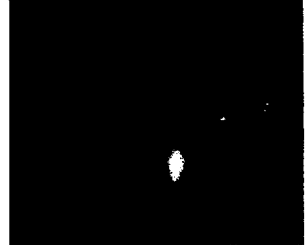
Sheared streamer  
 $t = t_0 + 2.5$  days



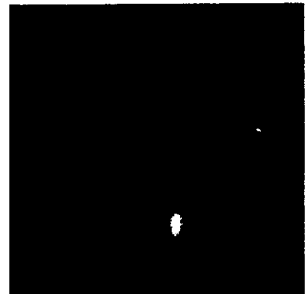
15% emerged flux  
 $t = t_0 + 2.5$  days



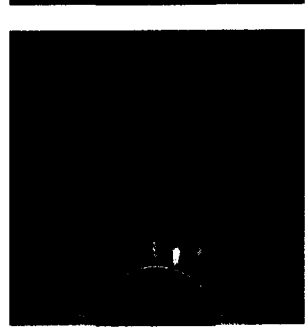
13.5% emerged flux  
 $t = t_0 + 18$  hours



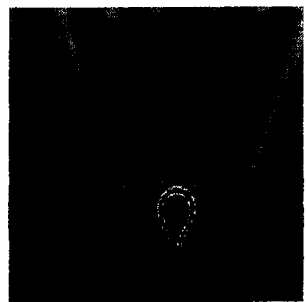
4.5% emerged flux  
 $t = t_0 + 6$  hours



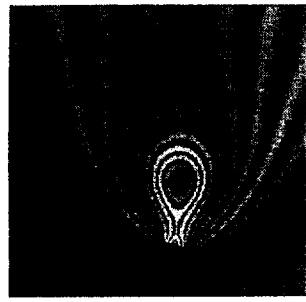
10.5% emerged flux  
 $t = t_0 + 16$  hours



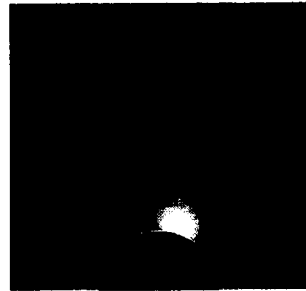
15% emerged flux  
 $t = t_0 + 20$  hours



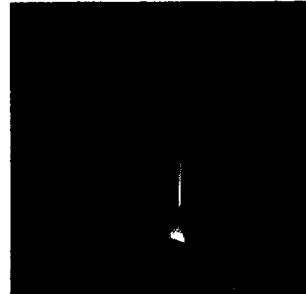
15% emerged flux  
 $t = t_0 + 2.5$  days



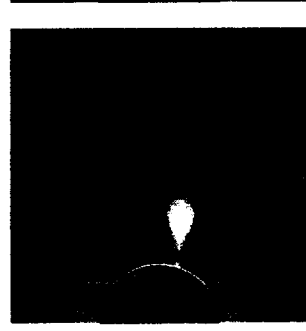
13.5% emerged flux  
 $t = t_0 + 20$  hours



4.5% emerged flux  
 $t = t_0 + 6$  hours



10.5% emerged flux  
 $t = t_0 + 16$  hours

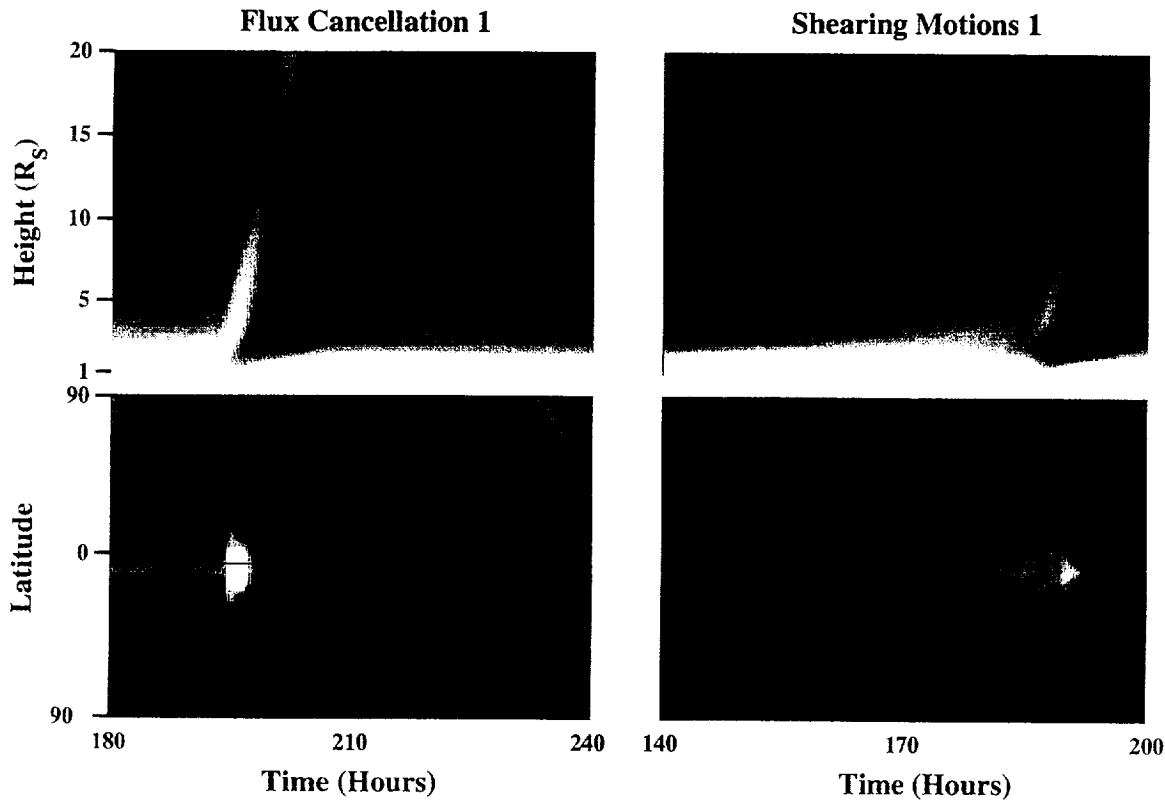


15% emerged flux  
 $t = t_0 + 20$  hours

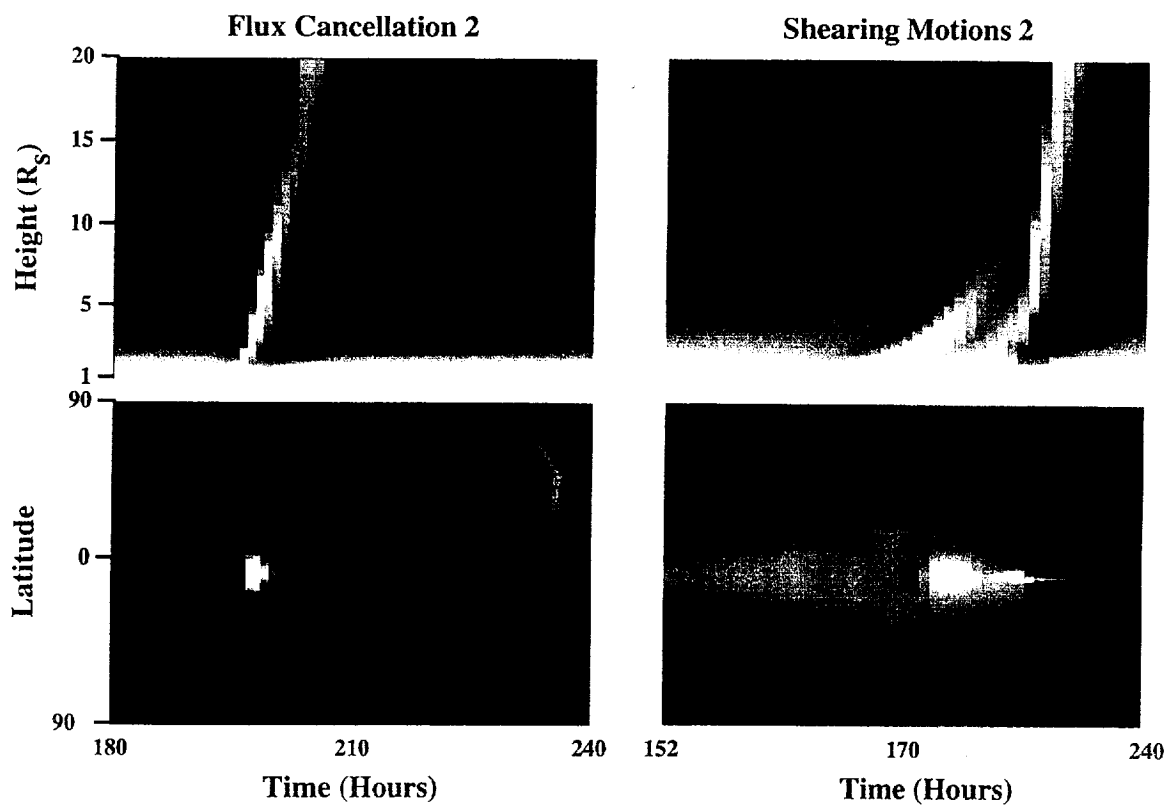


15% emerged flux  
 $t = t_0 + 2.5$  days

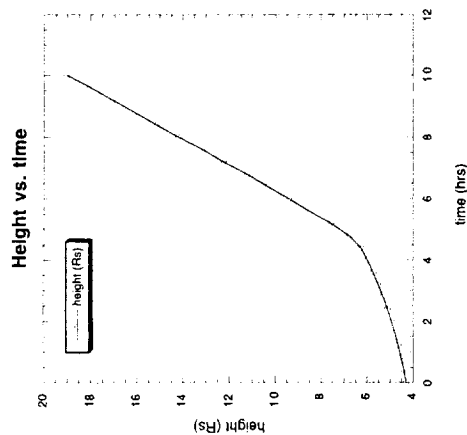
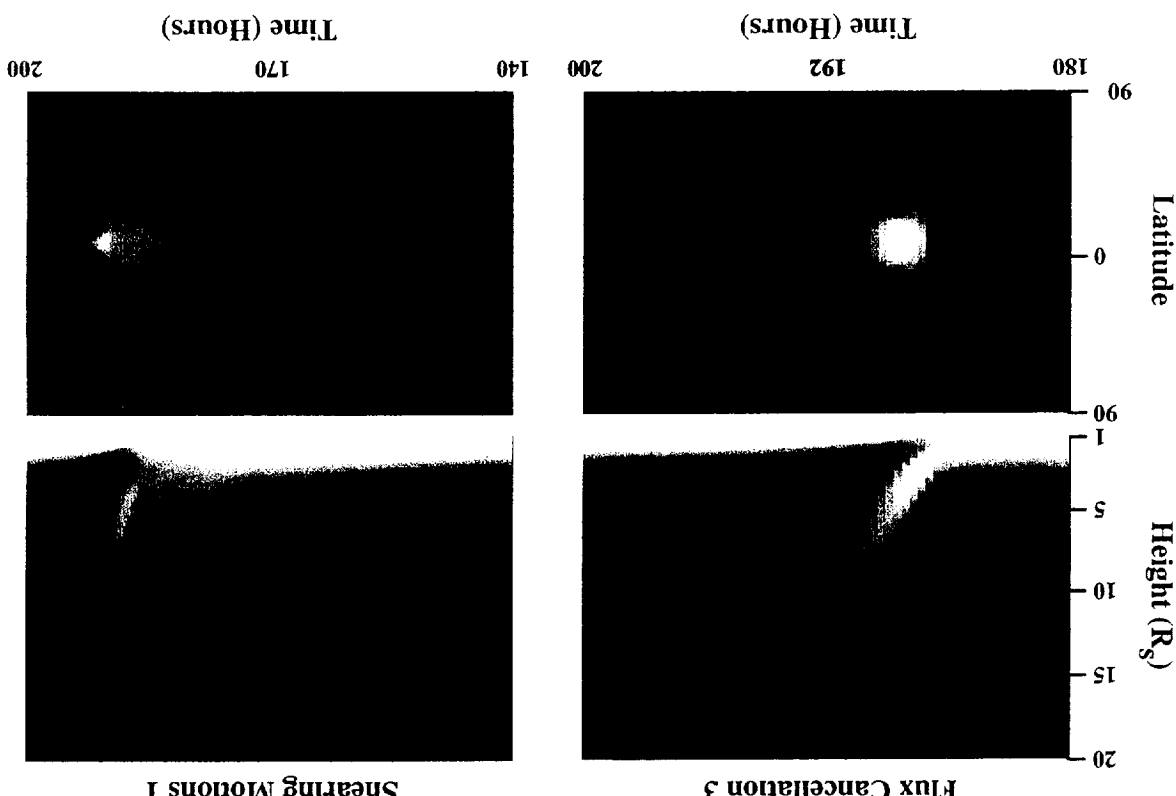
## TimeHeight Profiles: Flux Cancellation and Shearing Simulations



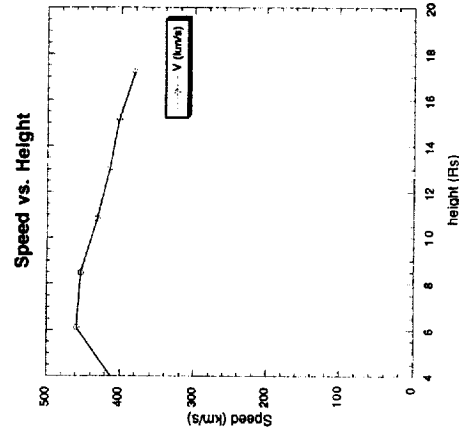
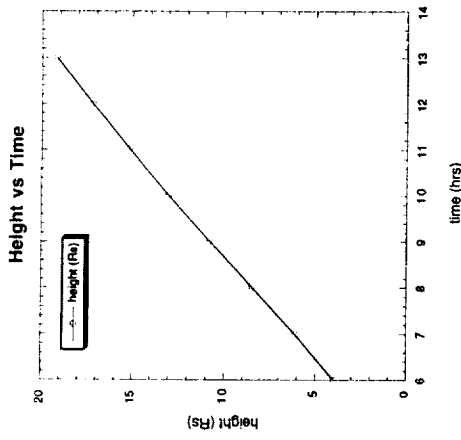
## TimeHeight Profiles: Slower Solar Wind



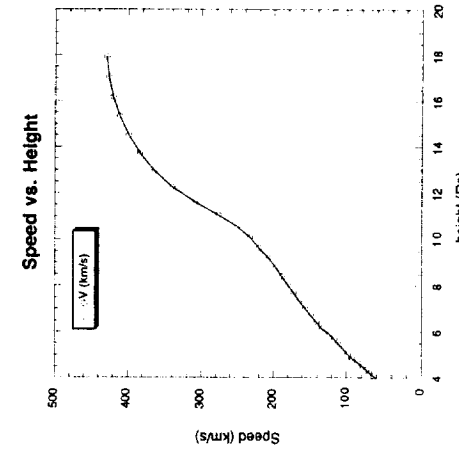
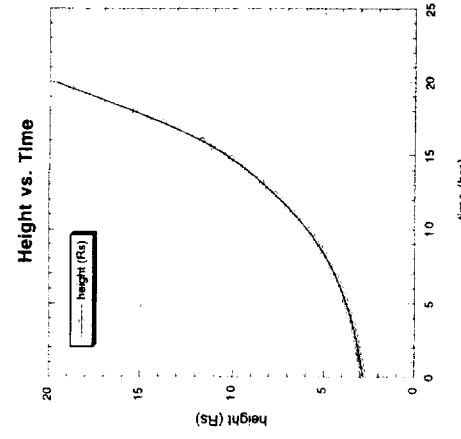
## Flux Cancellation, Medium Wind Background



## Flux Cancellation, Slow Wind Background

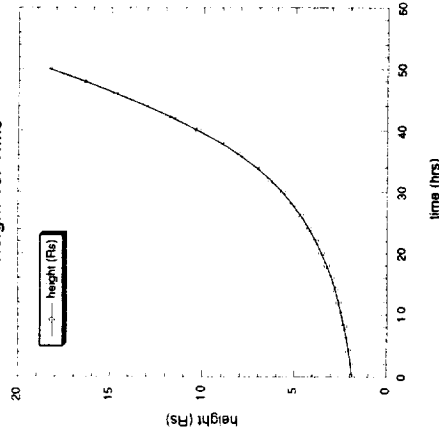


## Shearing Flows, Medium Wind

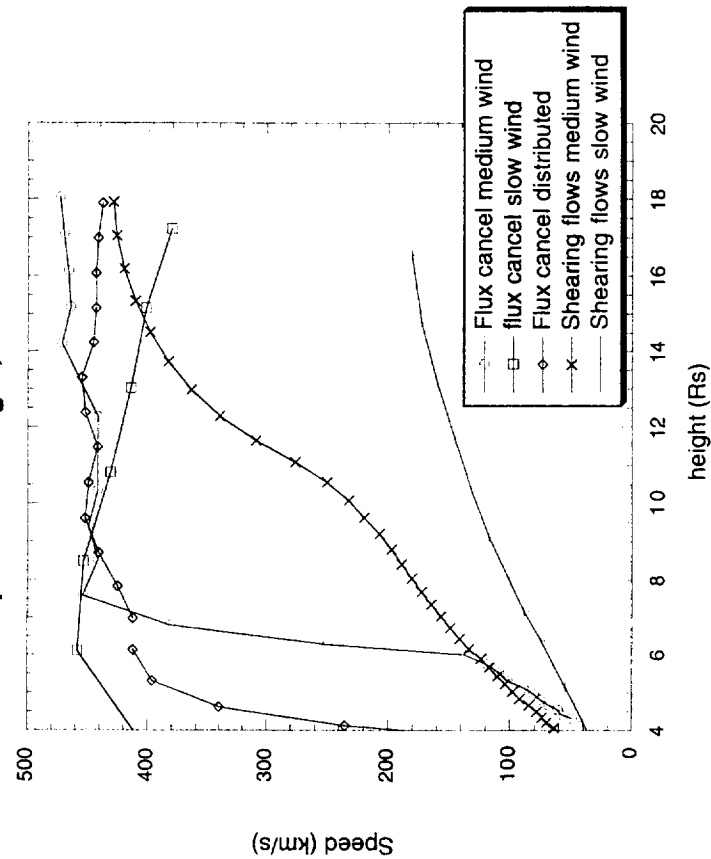


## Shearing Flows, Slow Wind

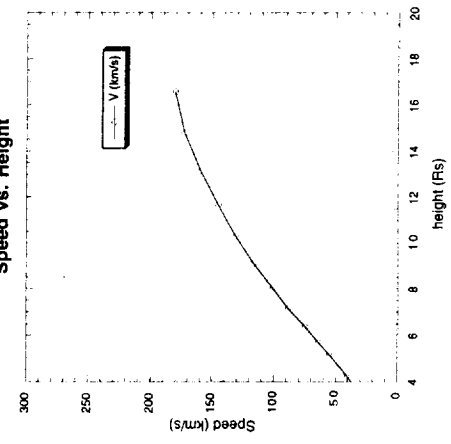
Height vs. Time



Speed vs. Height, 5 cases



Speed vs. Height



## SUMMARY

- We examined the results from simulated CMEs initiated by magnetic flux cancellation and by photospheric shearing flows.
- The flux cancellation CMEs yielded either accelerating or constant speed ejecta depending on the properties of the ambient solar wind.
- The CMEs initiated by photospheric shearing flows yielded accelerating ejecta. Shearing flow simulations with other initial configurations might also yield constant speed ejecta.

## WHAT HAVE WE LEARNED?

Questions I raised at the beginning of the talk:

- Does the rough division of CMEs into “accelerating” and “constant speed” imply more than one mechanism for CMEs initiation? No.
- Does this division imply that CMEs are initiated by only one mechanism? No.
- Can this classification *by itself* help us to understand CME initiation or constrain the possible mechanisms? No.
- Our results suggest that the approximate division of CMEs into “accelerating” or “constant speed” is a natural consequence of having a range of energy inputs and diverse solar wind conditions for different CME ejecta.

## **APPENDIX D**

“Using Global MHD Simulations to Interpret In Situ Observations of CMEs”

P. Riley, J. A. Linker, R. Lionello, Z. Mikić, D. Odstrcil, V. J. Pizzo,

T. H. Zurbuchen, and D. Lario

Presented at the Spring AGU Meeting

Boston, MA, May 29–June 2, 2001

# **Using Global MHD Simulations to Interpret in situ Observations of CMEs**

**Pete Riley, J. A. Linker, Z. Mikic**

SAIC, San Diego, California

**D. Odstrcil, V. J. Pizzo**

NOAA/SEC, Boulder, Colorado

**T. H. Zurbuchen**

University of Michigan

**D. Lario**

JHU/APL

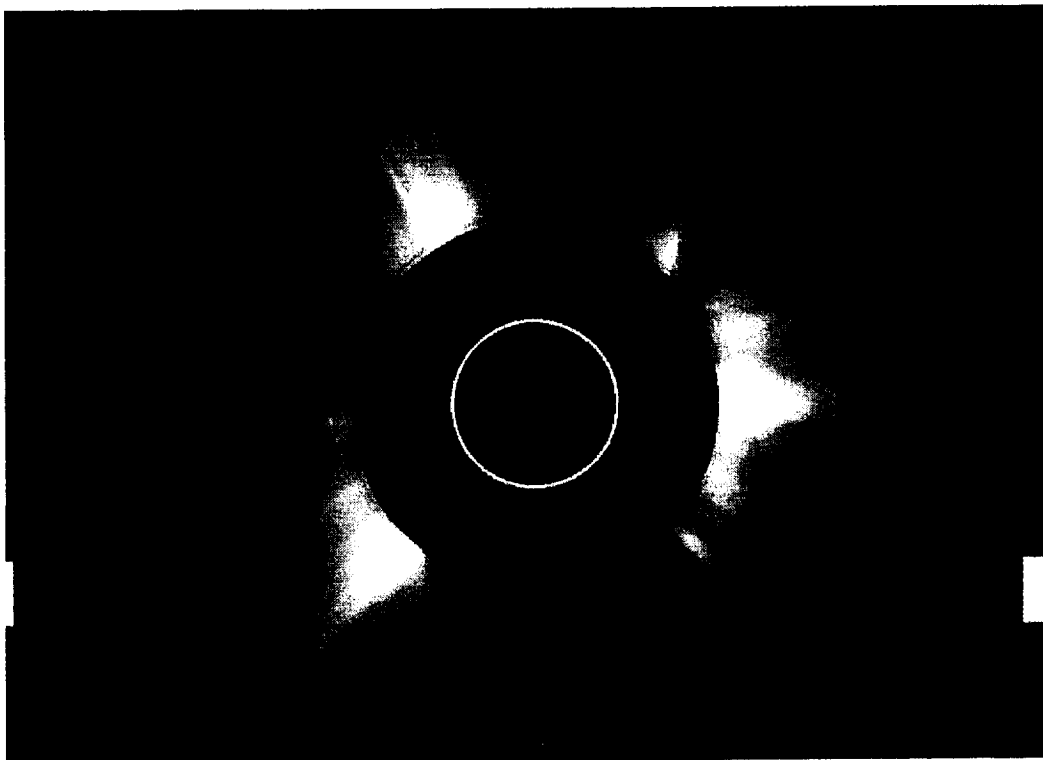
**R. P. Lepping**

NASA/Goddard

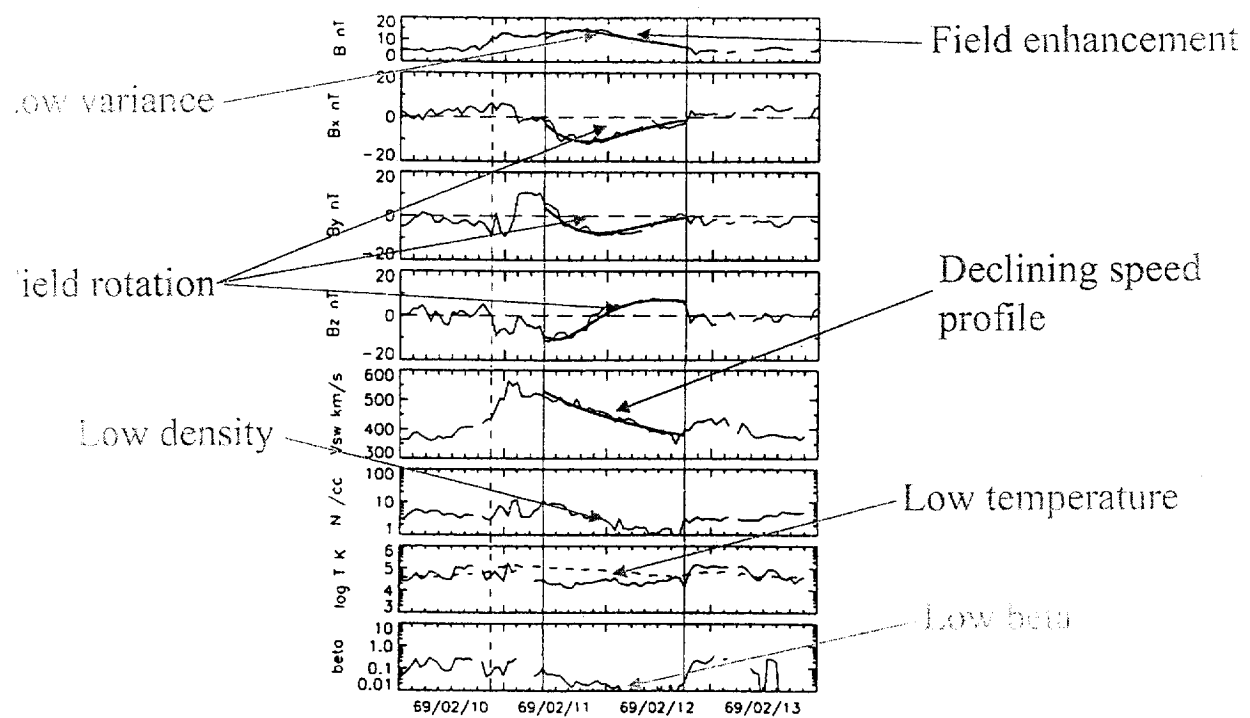
## **Overview**

- Introduction
  - Coronal observations of CMEs
  - In situ observations of magnetic clouds
  - Modeling Flux ropes
- MHD modelling of CMEs
  - Coronal model (SAIC)
  - Heliospheric model (NOAA/SEC)
- Comparison with observations
  - ACE/Ulysses spring 1999 event
- Summary
- Future work

# Introduction: White Light Observations of CMEs



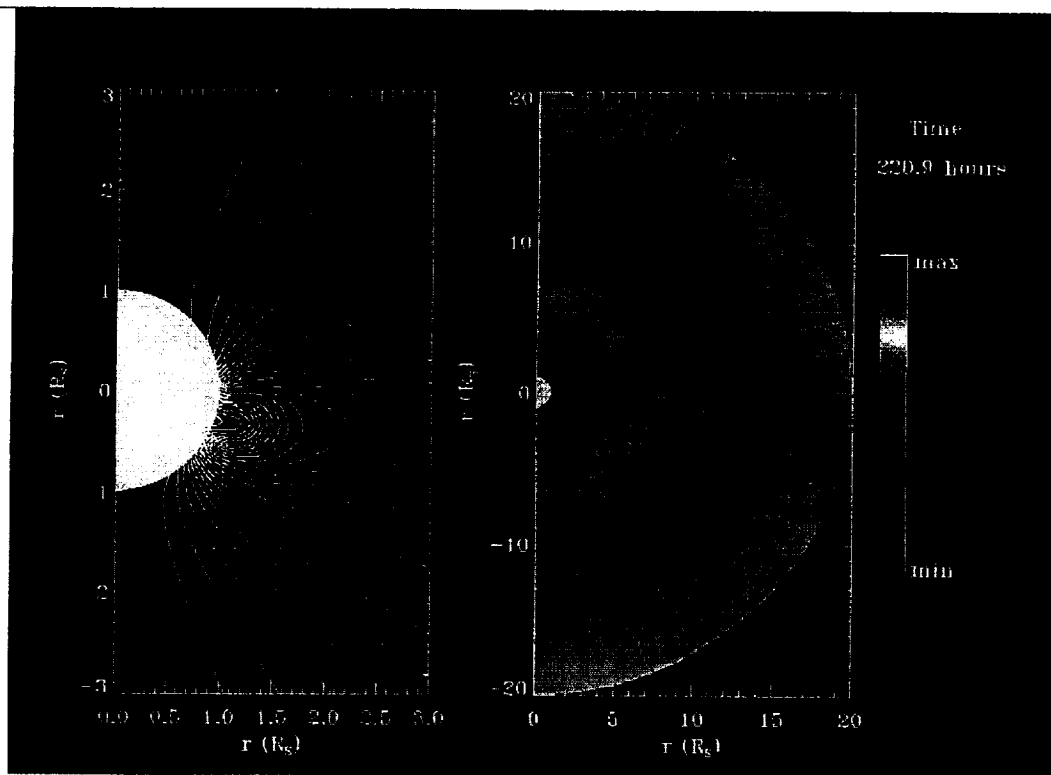
## Introduction: In situ observations of magnetic clouds



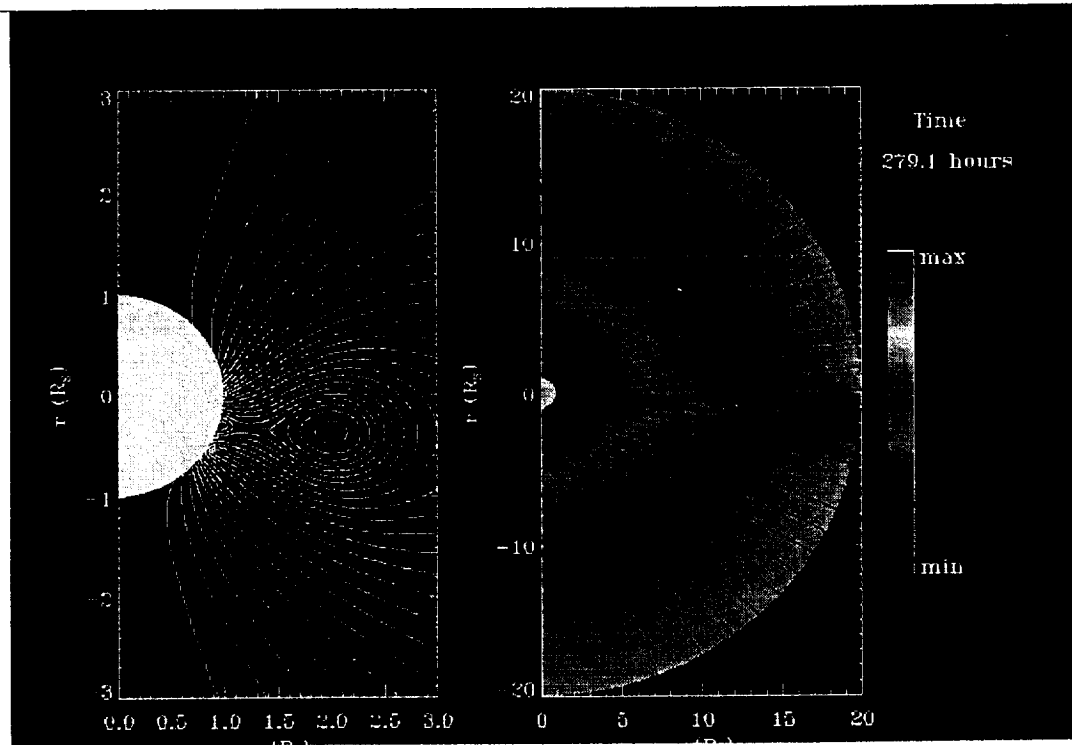
# Introduction: Models of Magnetic clouds/flux ropes

- Kinematic Models:
  - Force-free
  - Force-free with expansion
  - None force-free with expansion
- Dynamic Models:
  - Fluid
  - MHD

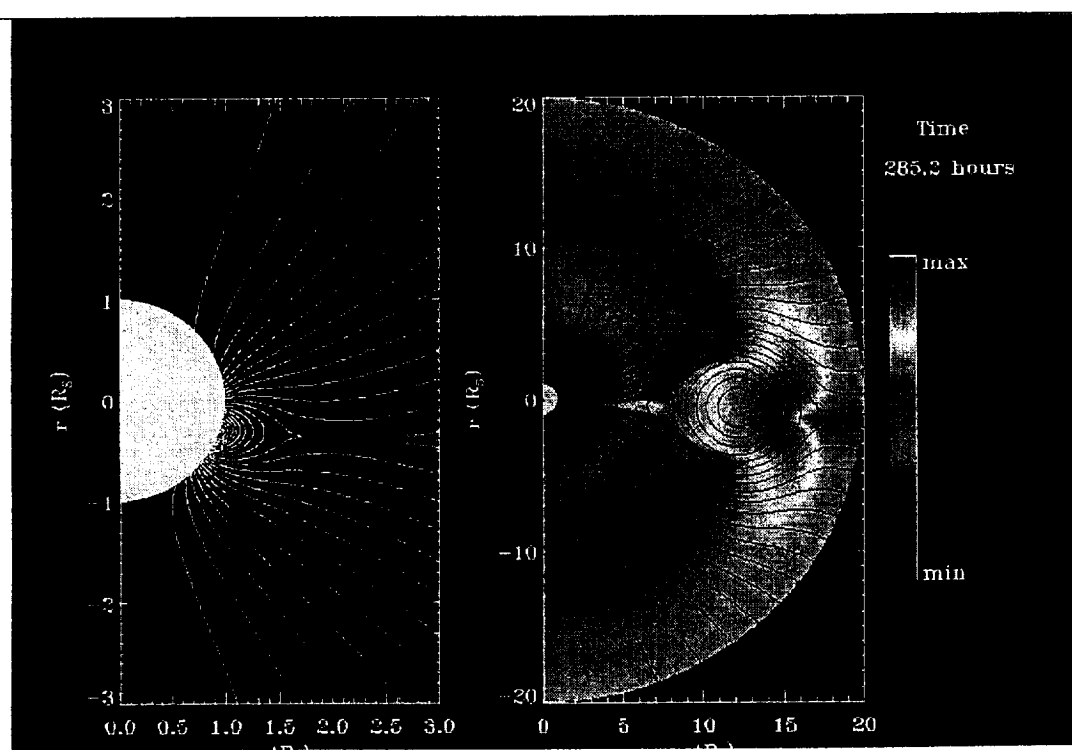
## MHD Simulation: Coronal solution



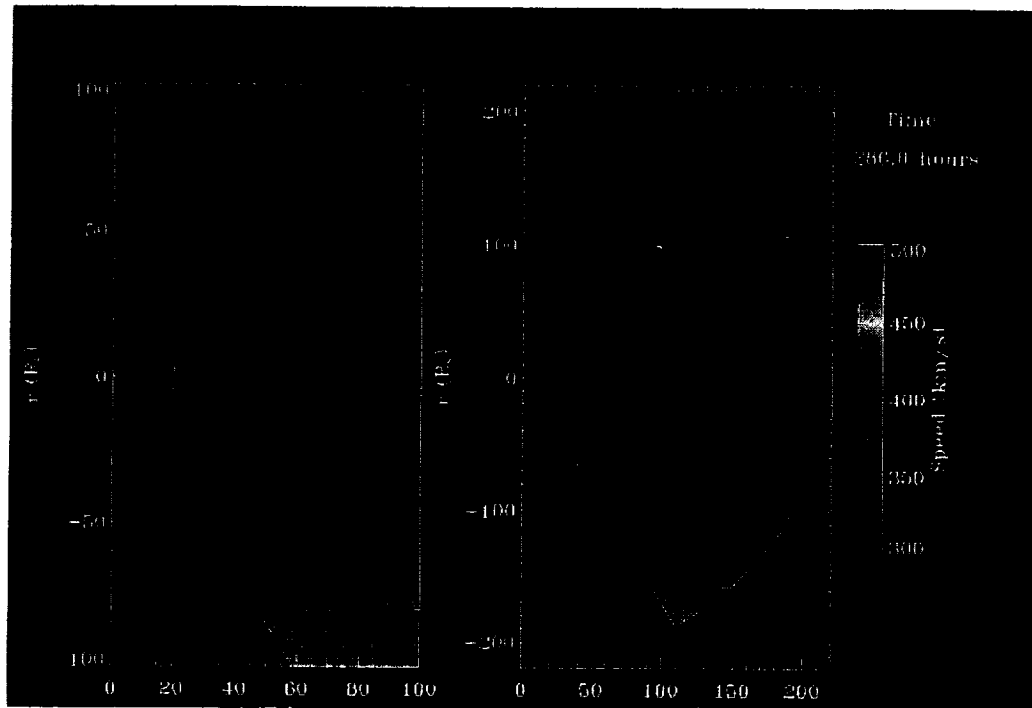
# MHD Simulation: Coronal solution



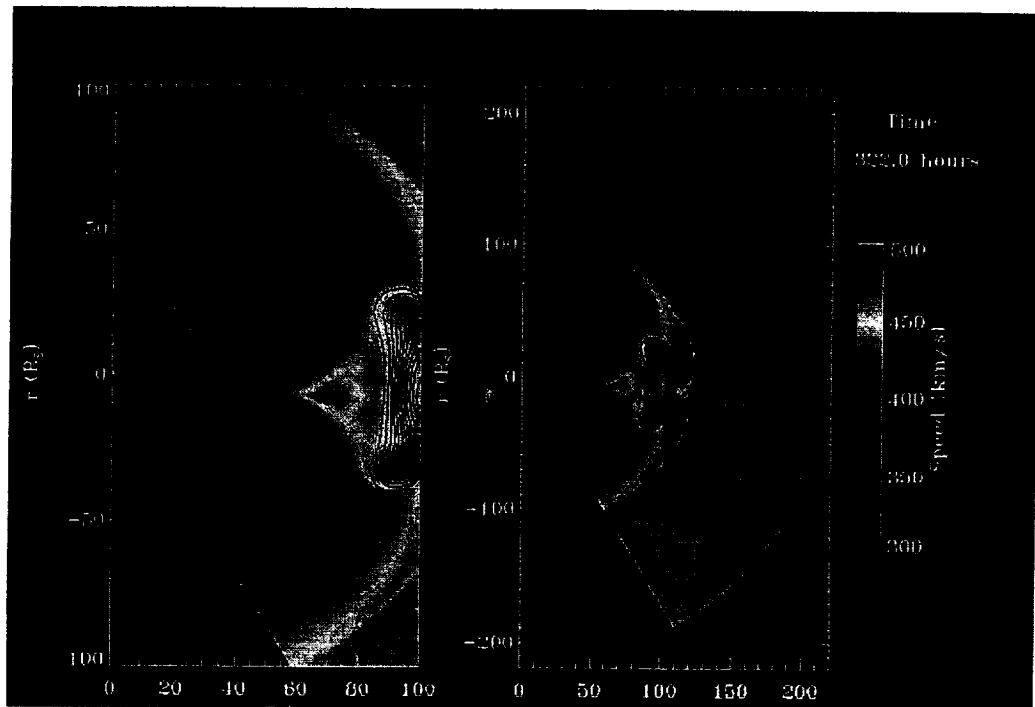
# MHD Simulation: Coronal solution



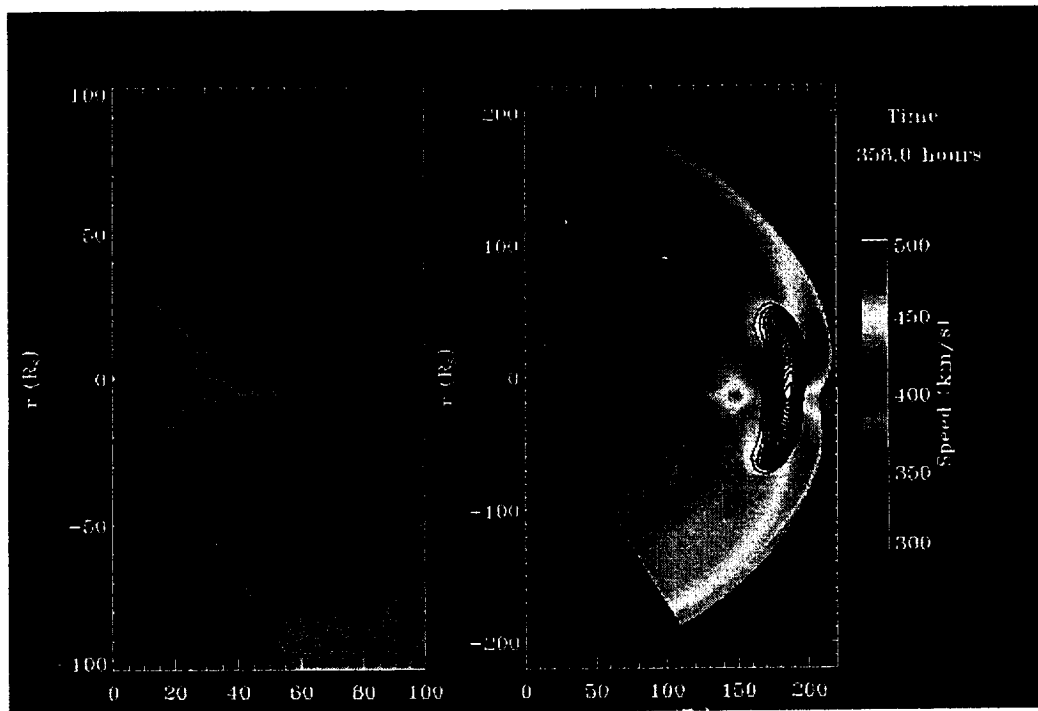
# MHD Simulation: Heliospheric solution



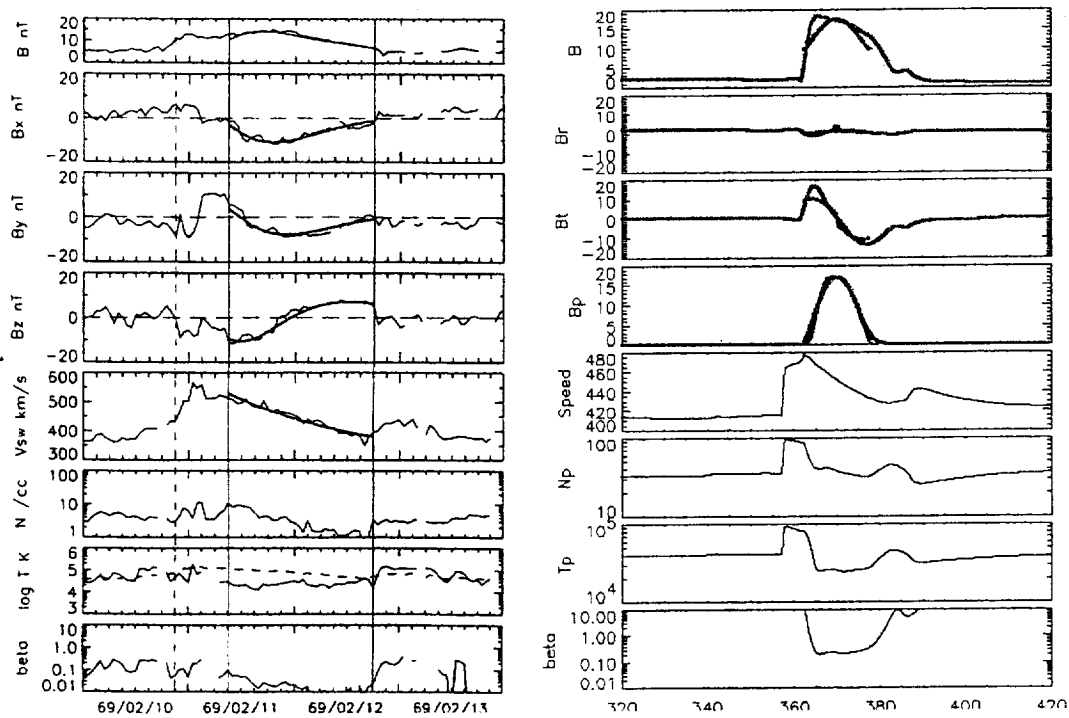
# MHD Simulation: Heliospheric solution



# MHD Simulation: Heliospheric solution

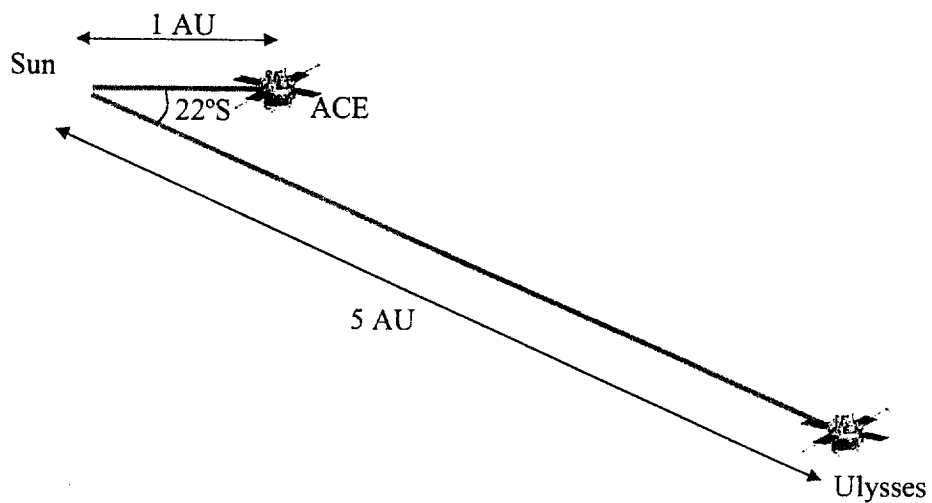


Comparison of an observed magnetic cloud  
with the generic simulation

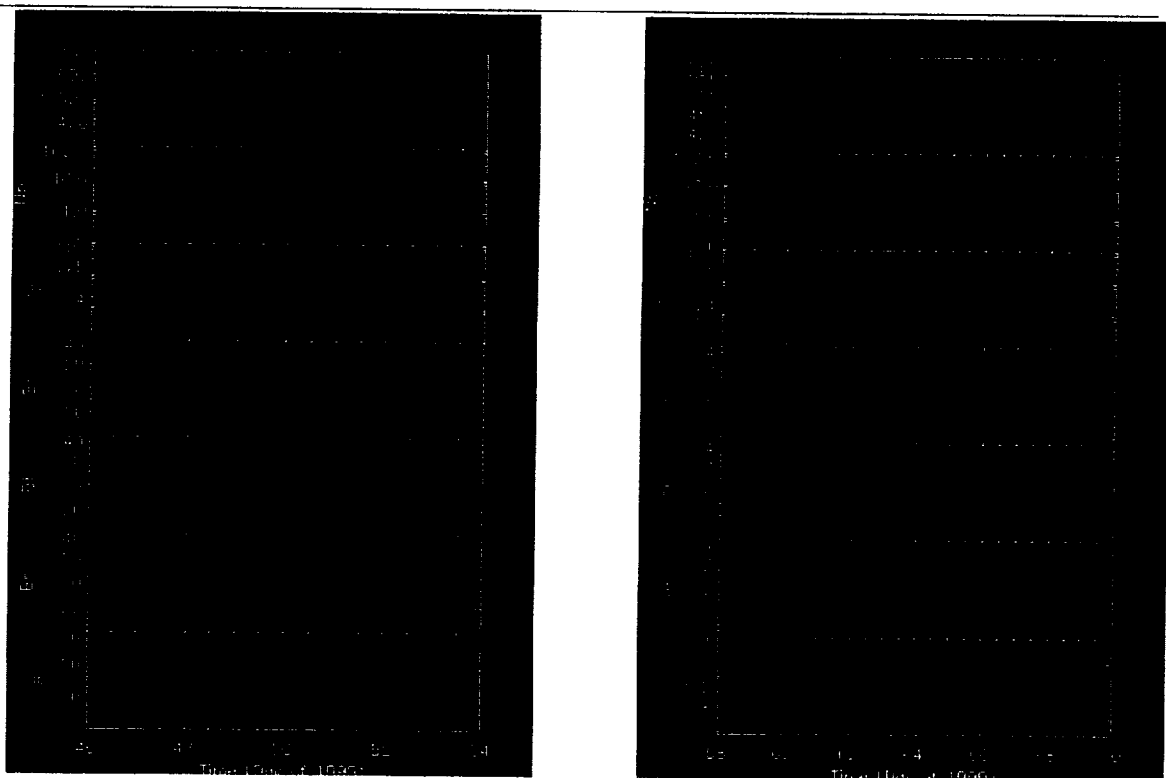


(Adapted from Marubashi, 1999)

# ACE/Ulysses Feb 1999 CME Event

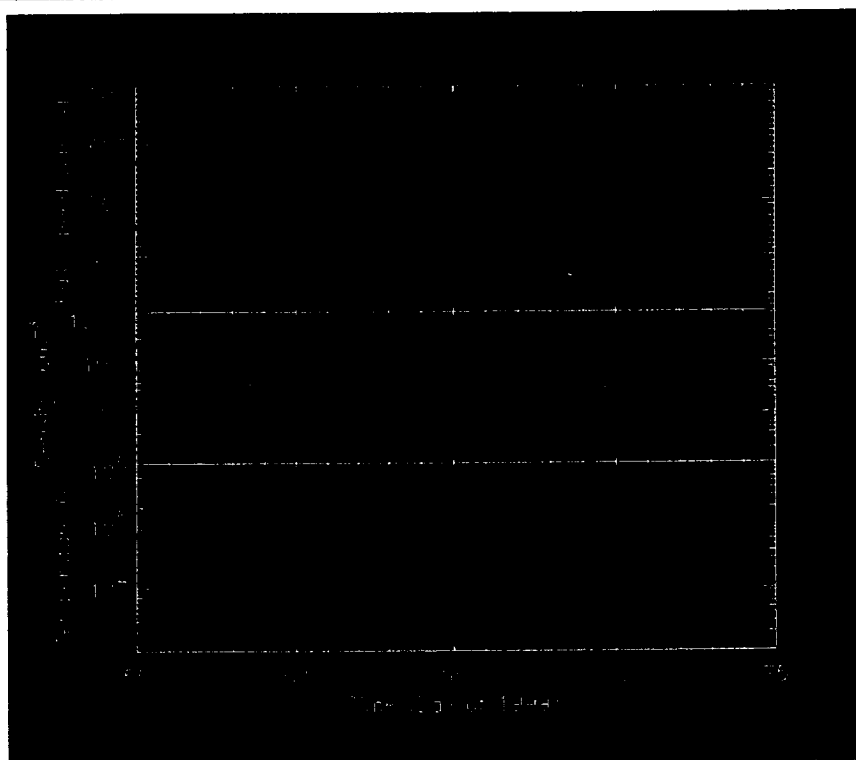


# ACE/Ulysses Feb 1999 CME Event



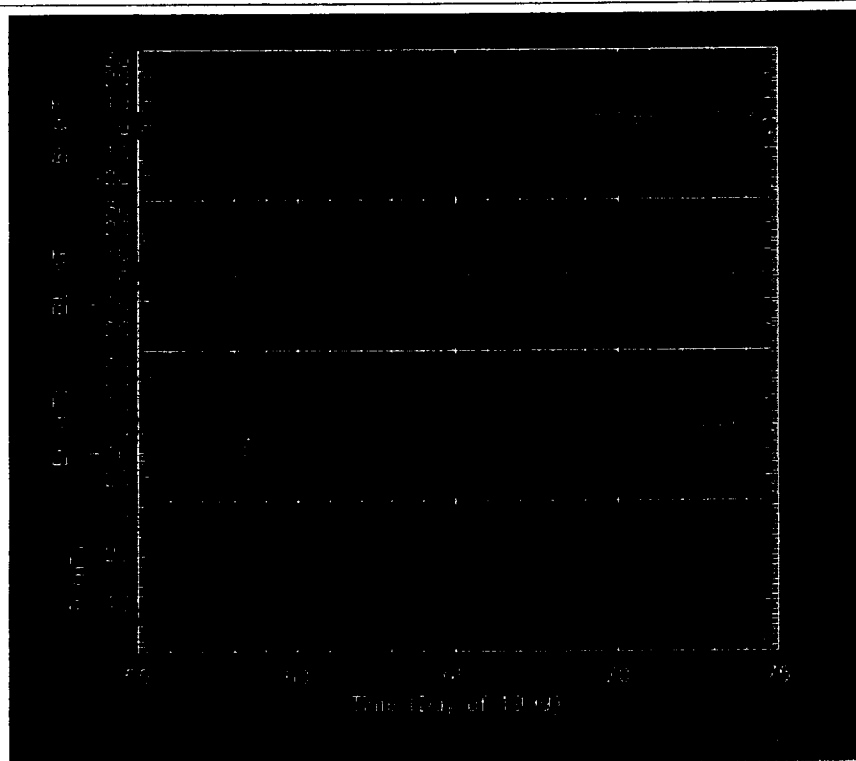
# **Ulysses/ACE May 1999 CME**

---



# **Ulysses/ACE May 1999 CME**

---



# Force-Free Fitting at ACE and Ulysses

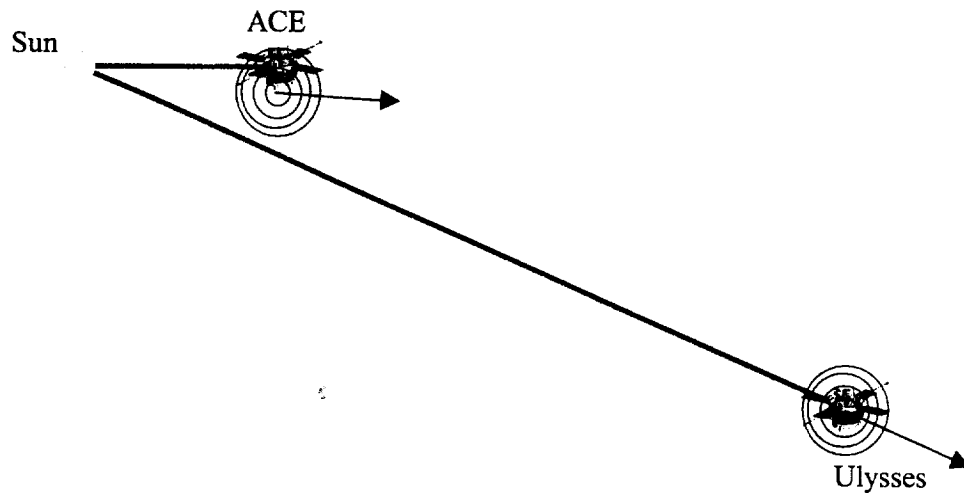
---

Parameter	ACE	Ulysses
<i>Start</i> (day hr:min)	49 14:00	62 20:00
<i>Stop</i> (day hr:min)	50 11:00	64 22:00
$\phi$ (deg)	282.1	271.1
$\theta$ (deg)	-1.3	53
$y/R$	0.738	0.0064
<i>Helicity</i>	-1	-1
$R$ (AU)	0.28	0.34

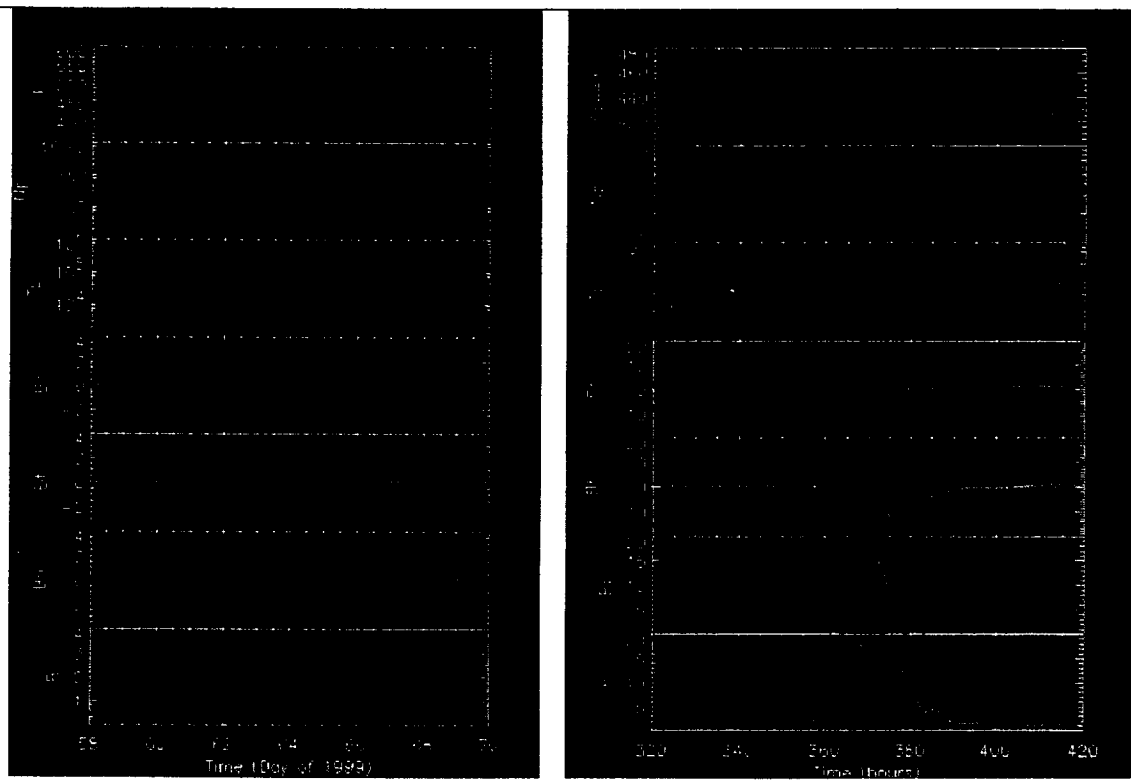
---

## ACE/Ulysses Feb 1999 CME Event: Global structure from force-free fitting

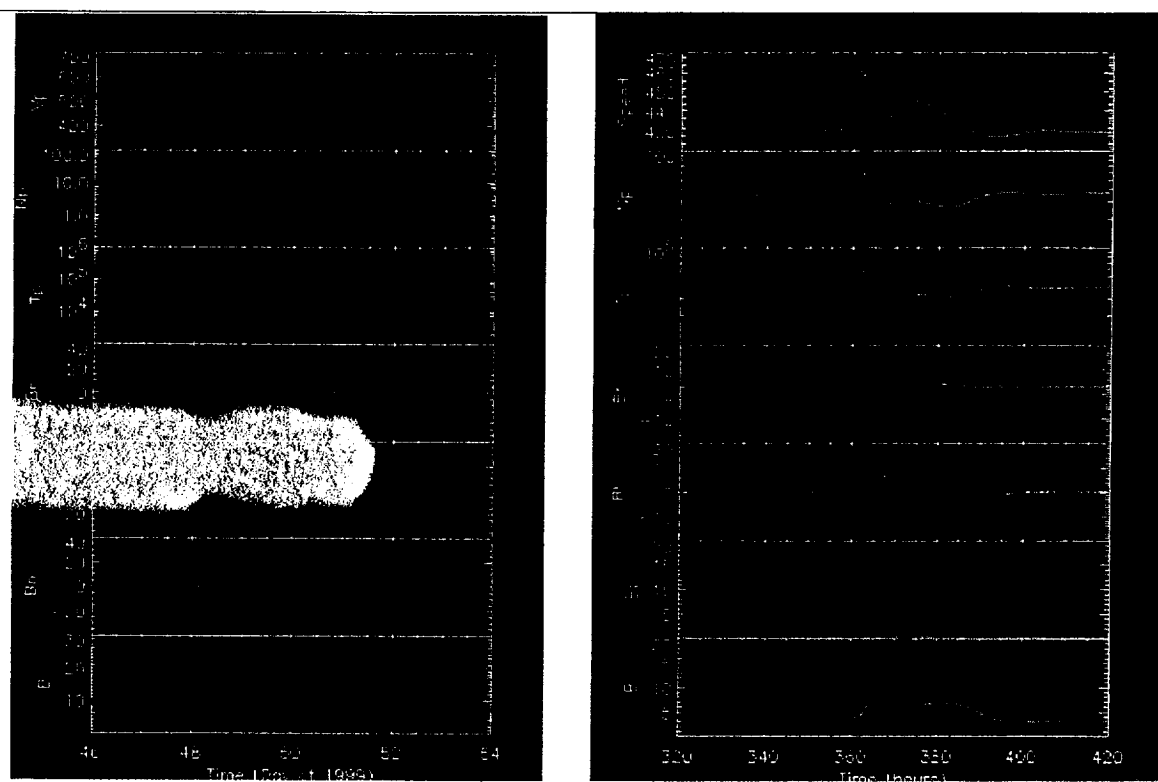
---



# Comparison of in situ observations with MHD simulation: Ulysses



# Comparison of in situ observations with MHD simulation: ACE



# Deceleration of CME

---

- Estimate time for CME to travel from ACE to Ulysses

$$V_{\text{CME}}(\text{ACE}) = 590 \text{ km/s}$$

$$V_{\text{CME}}(\text{Ulysses}) = 460 \text{ km/s}$$

Assume constant deceleration between 1 and 5 AU

$$\Rightarrow \Delta t = 13.62 \text{ days}$$

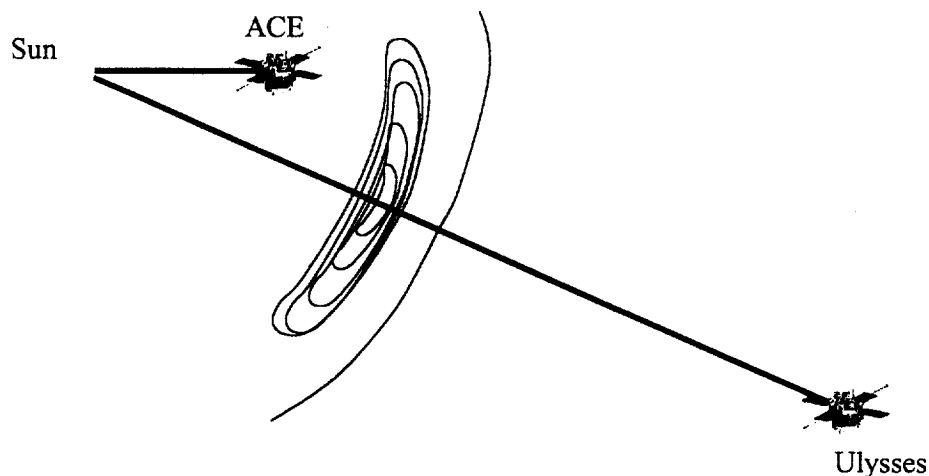
- CME actually arrived 13.9 days later

$\Rightarrow$  Large-scale structure not significantly distorted

---

## ACE/Ulysses Feb 1999 CME Event: Global structure

---



## **Summary**

---

- Idealized MHD simulations:
  - provide global context for interpreting in situ CME observations
  - Emphasize significant role of dynamics on the evolution of ejecta and their associated disturbances
  - Identify new effects that can be searched for in observations

---

## **Future Studies**

---

- Explore effects of different launch profiles
  - Do different mechanisms of eruptions lead to different interplanetary signatures?
- Launch CME in three dimensions
  - 3-D flow
  - Magnetic connectivity to Sun
- Incorporate composition into model

## **APPENDIX E**

**“Modeling of Transequatorial Loops with MH4D”**

R. Lionello and D. Schnack

Presented at the Spring AGU Meeting

Boston, MA, May 29–June 2, 2001

# Modeling of Transequatorial Loops with MH4D

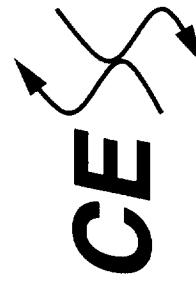
## GOALS AND CHALLENGES

- Develop an efficient 3-D discrete representation for the resistive MHD model using an unstructured grid of tetrahedral cells
  - Truly arbitrary geometry
  - Use Cartesian coordinates
  - Avoids coordinate singularities and complicated metrics
- Apply to a variety of problems
  - Fusion
  - Solar and space physics
  - ??
- Challenges
  - Discrete representation of differential operators
    - Compactness (couple only nearest neighbor grid points)
    - Self-adjointness
    - Annihilation properties (eg.,  $\nabla \cdot \mathbf{B} = 0$ )
  - Solution of implicit system
    - Grid generation
    - Implementation
      - Code and data structure (OO techniques)
      - Parallelism
      - Grid decomposition

R. Lionello

and

D. D. Schnack



Center for Energy and Space Science  
San Diego, CA



## THE FIRST CHALLENGE

Find efficiently computable discrete representations of the magnetic field and differential operators on a 3-D unstructured grid of tetrahedra

- The magnetic field and current density:

$$\mathbf{B} = \nabla \times \mathbf{A}, \quad \mathbf{J} = \nabla \times \mathbf{B},$$

$$\mathbf{J} = \nabla \times \nabla \times \mathbf{A}$$

and consequently

- Both  $\mathbf{B}$  and  $\mathbf{J}$  are solenoidal

- The operator is self-adjoint:  
provided  $\mathbf{A}_1$  and  $\mathbf{A}_2$  satisfy the same boundary

$$\int \mathbf{A}_2 \cdot \nabla \times \nabla \times \mathbf{A}_1 dV = \int \mathbf{A}_1 \cdot \nabla \times \nabla \times \mathbf{A}_2 dV$$

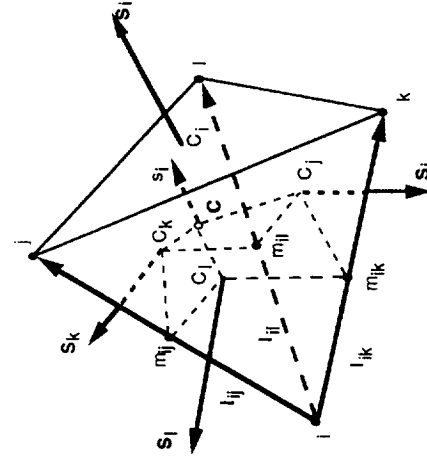
conditions

- Seek a discrete representation that retains these properties

- Sides are labeled by the index of their opposite vertex.
- $\mathbf{C}$  is the centroid of the tetrahedron.
- $\mathbf{m}_{ij}$  is the midpoint of edge  $ij$ .
- $\mathbf{C}_i$  is the centroid of side  $i$ .
- $\mathbf{s}_i$  is the vector area of side  $i$ .
- $\mathbf{m}_{ij}$ ,  $\mathbf{C}_i$ ,  $\mathbf{C}$ , and  $\mathbf{C}_k$  are coplanar.
- $s_i$  is the area of the dual median surface.

$$s_i = s_i / 3$$

## GEOMETRY



## FINITE VOLUME METHOD

- Use integral relations to define differential operators

- Examples:  
Gradient:

$$\int \nabla f dV = \int_S \hat{n} f dS$$

Divergence:

$$\int \nabla \cdot \mathbf{F} dV = \int_S \hat{n} \cdot \mathbf{F} dS$$

Curl (2-D):

$$\int_S \hat{n} \cdot \nabla \times \mathbf{F} dS = \oint_C \mathbf{F} \cdot d\mathbf{l}$$

Curl (3-D):

$$\int \nabla \times \mathbf{F} dV = \int_S \hat{n} \times \mathbf{F} dS$$

- Integrate over control volume (computational cell), eg.,

$$(\nabla f)_c = \frac{1}{V_c} \sum_s \hat{n}_s f_s S_s$$

- We will apply this technique to tetrahedral and dual median volume elements

## THE MAGNETIC FIELD

- The vector potential  $\mathbf{A}$  is defined at vertices of tetrahedra

$\mathbf{A}$  varies linearly within a tetrahedron

- Integral definition:

$$\int \mathbf{B} dV = \int \nabla \times \mathbf{A} dV = \int_S \mathbf{S} \times \mathbf{A}$$

- Apply to tetrahedral cell:

$$\mathbf{B}_\tau V_\tau = \sum_{s=1}^4 \mathbf{S}_s \times \bar{\mathbf{A}}_s$$

- $\mathbf{B}_\tau$  is constant within tetrahedron  $\tau$

$\bar{\mathbf{A}}_s$  is the average of  $\mathbf{A}$  over the 3 vertices of side  $S$

$V_\tau$  is the volume of tetrahedron  $\tau$

- In terms of vertices

$$\mathbf{B}_\tau = -\frac{1}{3V_\tau} \sum_{v(\tau)} \mathbf{S}_v \times \mathbf{A}_v$$

$v(\tau)$  are the indices of the 4 vertices of tetrahedron  $\tau$

$\mathbf{S}_v$  is the (outward directed) side opposite vertex  $v$

## DIVERGENCE OF B

- Apply Gauss' theorem to dual median volume element surrounding vertex  $v$

$$V_v = \sum_{\tau(v)} \frac{1}{3} V_\tau \text{ is the volume of this cell}$$

$\tau(v)$  are the indices of the tetrahedra sharing vertex  $v$

$$(\nabla \cdot \mathbf{B})_v V_v = \frac{1}{3} \sum_{\tau} \mathbf{B}_\tau \cdot \mathbf{S}_{v(\tau)}$$

$$= \frac{1}{3} \sum_{\tau} \frac{1}{V_\tau} \sum_{\gamma(\tau)} \bar{\mathbf{A}}_\gamma \cdot (\mathbf{s}_v \times \mathbf{s}_\gamma)$$

$v(\tau)$  is the index of the side of tetrahedron  $\tau$  opposite vertex  $v$

$\gamma(\tau)$  are the indices of the 4 sides of tetrahedron  $\tau$

- This gives:

- NOW A MIRACLE OCCURS!!

After some algebra, we find that the contributions from common faces of adjoining tetrahedra cancel exactly!

- The result!

$$(\nabla \cdot \mathbf{B})_v = 0$$

- **Caveat:** This holds for interior vertices only

## ALTERNATE DERIVATION OF B

- $\mathbf{A}(x)$  varies linearly within a tetrahedron:
- Take the curl of this function in tetrahedron  $\tau$ .

$$\mathbf{A}(x) = \sum_v \mathbf{A}_v \left[ 1 - \frac{1}{3V_\tau} \mathbf{S}_v \cdot (\mathbf{x} - \mathbf{x}_v) \right]$$

- The result is:

$$\mathbf{B}_\tau = -\frac{B_\alpha}{3V_\tau} \sum_{\gamma \neq \alpha} \frac{\partial A_\gamma}{\partial A_\alpha}$$

- Identical to the finite-volume expression!

- Demonstrates first order accuracy (exact for linear functions)
- Have been unable to show second order accuracy

## THE CURRENT DENSITY

- Use generalized Stokes' formula as applied to dual median volume element

$$\int \mathbf{J} dV = \int \nabla \times \mathbf{B} dV = \int_S \hat{\mathbf{n}} \times \mathbf{B} dS$$

$$\mathbf{J}_v V_v = \frac{1}{3} \sum_{\tau(v)} \mathbf{S}_{v(\tau)} \times \mathbf{B}_\tau$$

$$\mathbf{J}_v V_v = \sum_{\tau(v)v'(\tau)} \sum \mathbf{M}^\tau(v, v') \cdot \mathbf{A}_{v'}$$

$$\mathbf{M}^\tau(v, v') = \frac{1}{9V_\tau} [(\mathbf{S}_{v(\tau)} \cdot \mathbf{S}_{v'(\tau)}) - \mathbf{S}_{v(\tau)} \mathbf{S}_{v'(\tau)}]$$

- Substituting the expression for  $\mathbf{B}$  in terms of  $\mathbf{A}$ :

- Symmetry:

$$M_{\alpha\beta}^\tau(v, v') = M_{\beta\alpha}^\tau(v', v), \quad \alpha, \beta = x, y, z$$

- This is the discrete "curl-curl" operator

## SELF-ADJOINTNESS

- Define inner product:

$$(\mathbf{P}, \mathbf{Q}) = \int \mathbf{P} \cdot \mathbf{Q} dV = \sum_{\tau=1}^{N_t} \sum_{v(\tau)} \frac{1}{4} V_\tau \mathbf{P}_v \cdot \mathbf{Q}_v$$

- $L$  is self-adjoint if:

$$(\mathbf{P}, L \cdot \mathbf{Q}) = (\mathbf{Q}, L \cdot \mathbf{P})$$

- Direct calculation using symmetry of  $\mathbf{M}$ :

$$\begin{aligned} (\mathbf{P}, \mathbf{M} \cdot \mathbf{Q}) &= \sum_{\tau} \frac{1}{4} V_\tau \sum_v \sum_{v'} \mathbf{P}_v \cdot \mathbf{M}^\tau(v, v') \cdot \mathbf{Q}_{v'} \\ &= \sum_{\tau} \frac{1}{4} V_\tau \sum_v \sum_{v'} \mathbf{Q}_{v'} \cdot \mathbf{M}^\tau(v', v) \cdot \mathbf{P}_v \\ &= \sum_{\tau} \frac{1}{4} V_\tau \sum_v \sum_{v'} \mathbf{Q}_{v'} \cdot \mathbf{M}^\tau(v', v) \cdot \mathbf{P}_v \\ &= (\mathbf{Q}, \mathbf{M} \cdot \mathbf{P}) \end{aligned}$$

- The discrete operator is self-adjoint

## VARIATIONAL PRINCIPLE

- **Minimize functional**

$$I(\mathbf{A}) = \frac{1}{2} \int [(\nabla \times \mathbf{A})^2 - 2\mathbf{J} \cdot \mathbf{A}] dV$$

- **Variation of  $\mathbf{A}$ :** let

$$\mathbf{A} \rightarrow \mathbf{A} + \varepsilon \delta \mathbf{A}$$

$$\begin{aligned} I(\mathbf{A} + \varepsilon \delta \mathbf{A}) &= \frac{1}{2} \int [(\nabla \times \mathbf{A})^2 - 2\mathbf{J} \cdot \mathbf{A}] dV \\ &\quad + \varepsilon \int (\nabla \times \mathbf{A} \cdot \nabla \times \delta \mathbf{A} - \mathbf{J} \cdot \delta \mathbf{A}) dV \\ &\quad + \frac{1}{2} \varepsilon^2 \int (\nabla \times \delta \mathbf{A})^2 dV \end{aligned}$$

- **For minimum, coefficient of  $\varepsilon$  must vanish:**

$$\int \delta \mathbf{A} \cdot (\nabla \times \nabla \times \mathbf{A} - \mathbf{J}) dV = - \int_S \delta \mathbf{A}_t \cdot (\mathbf{B} \times \hat{\mathbf{n}}) dS$$

$$\mathbf{A}_t = (\mathbf{I} - \hat{\mathbf{n}}\hat{\mathbf{n}}) \cdot \mathbf{A}$$

- **Natural boundary condition:**

$$\delta \mathbf{A}_t = 0, \text{ or } \mathbf{A}_t \text{ specified on boundary (Dirichlet)}$$

- **Solutions**  $\nabla \times \nabla \times \mathbf{A} = \mathbf{J}$ , with  $\mathbf{J}$  specified in  $V$ , and  $\mathbf{A}_t$  specified on the boundaries, minimize  $I(\mathbf{A})$ .

## DISCRETE MINIMIZATION

- Minimize  $I(\mathbf{A})$  on a grid with  $N_v$  vertices and  $N_t$  tetrahedra
- Expand  $\mathbf{A}(\mathbf{x})$  in basis functions

$$\mathbf{A}(\mathbf{x}) = \sum_v \mathbf{A}_v \alpha_v(\mathbf{x})$$

- Expand  $\mathbf{J}$  in delta-functions

$$\mathbf{J}(\mathbf{x}) = \sum_v V_v \mathbf{J}_v \delta(\mathbf{x} - \mathbf{x}_v)$$

- Substitute into  $I(\mathbf{A})$ :

$$I = \frac{1}{2} \sum_v \sum_{v'} [\mathbf{A}_v \cdot \mathbf{M}(v, v') \cdot \mathbf{A}_{v'} - V_v \mathbf{J}_v \cdot \mathbf{A}_{v'} \alpha_{v'}(\mathbf{x}_{v'})]$$

$$\mathbf{M}(v, v') = \int [(\nabla \alpha_v \cdot \nabla \alpha_{v'})] - \nabla \alpha_v \cdot \nabla \alpha_{v'} dV$$

- To minimize, set

$$\frac{\partial I}{\partial A_{\gamma, v}} = 0, \quad \gamma = x, y, z$$

- Result:

$$\left( \sum_v \alpha_\mu(\mathbf{x}_v) \right) V_v \mathbf{J}_v = \sum_\tau \sum_v \mathbf{M}^\tau(\mu, v) \cdot \mathbf{A}_{v'}, \quad \mathbf{M} = \sum_\tau \mathbf{M}^\tau$$

- With tent expansion functions ( $\alpha_\mu(\mathbf{x}_v) = \delta_{\mu, v}$ ), gives finite volume expression

## BOUNDARY CONDITIONS

- No reference to boundary conditions in discrete minimization
- Discrete expression for the “curl-curl” operator is  $3N_v$  equations in  $3N_v$  unknowns  
*Could be solved for all unknowns, including all values at the  $M_v$  boundary vertices*
- Absence of surface term implies that solution will satisfy the natural boundary condition

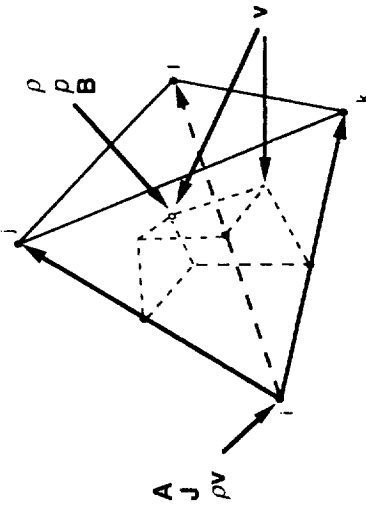
$$\delta \mathbf{A}_t \cdot (\mathbf{B} \times \hat{\mathbf{n}}) = 0$$

- Since  $\mathbf{A}_t$  is not fixed, this can be satisfied only if  $\mathbf{B} \times \hat{\mathbf{n}} = 0$
- Constraint on source and surface field:  
*Solutions with vanishing tangential magnetic field*  
$$\int_S \delta \mathbf{A}_t \times \mathbf{B} = \int \mathbf{J} dV$$
*exist only if total current vanishes*
- In general, we must specify  $\mathbf{A}_t$  on the boundary

## ALTERNATE BOUNDARY CONDITIONS

- Must include surface term in the functional to be minimized
- $$I(\mathbf{A}) = \int [(\nabla \times \mathbf{A})^2 - 2\mathbf{J} \cdot \mathbf{A}] dV + \int_S (\mathbf{A}_t \cdot \mathbf{P} - 2\mathbf{Q}) \cdot \mathbf{A}_t dS$$
- $P$  is a self-adjoint matrix and  $Q$  is a vector
- Performing variation and minimization as before leads to the condition
- $$\int \delta \mathbf{A} \cdot (\nabla \times \nabla \times \mathbf{A} - \mathbf{J}) dV + \int \delta \mathbf{A}_t \cdot (\mathbf{B} \times \hat{\mathbf{n}} + \mathbf{P} \cdot \mathbf{A}_t - \mathbf{Q}) dS = 0$$
- Since the tangential variation no longer vanishes at the surface, this can be satisfied only if
- Mixed (von Neumann/Dirichlet) boundary condition
- $$\nabla \times \nabla \times \mathbf{A} = \mathbf{J} \text{ in } V, \text{ and } \mathbf{B} \times \hat{\mathbf{n}} + \mathbf{P} \cdot \mathbf{A}_t = \mathbf{Q} \text{ on } S$$
- Allows specification of tangential magnetic field
  - Could apply discrete minimization to this modified functional to obtain more formalism that accommodates these boundary conditions

## MHD FORMULATION



- Vertices:

- $A$ ,  $J$ , and  $\rho v$

- Centroids:

- $\rho$ ,  $\rho v$ , and  $B$

- Velocity averaged to faces or centroids, as required

- All quantities advanced in time by applying conservation laws to control volume

- Use the NIMROD anisotropic semi-implicit operator

## SUMMARY AND STATUS

- Developed a formalism for defining  $A$ ,  $B$ , and  $J$  on an unstructured grid of tetrahedra
- Finite-volume approach
- $B$  is solenoidal
- “curl-curl” operator is compact and self-adjoint
- Solutions of discrete equations minimize the same functional as solutions of differential equations
- Tangential  $A$  can be specified on boundary
  - Can be generalized to specify tangential  $B$
- Caveats:
  - Demonstrated only first order accuracy
  - $B$  is solenoidal only on interior vertices
    - Have not demonstrated that  $J$  is solenoidal
  - Solved model implicit resistive diffusion problem
  - Starting point for full MHD model

## PRELIMINARY VALIDATION

- Successive application of  $\nabla \times$  operators on primary and dual grids is identical to the composite  $\nabla \times \nabla \times$  operator

- Verified that  $\nabla \cdot \mathbf{B} = 0$

- Solution of diffusion equation in cubic, cylindrical, and spherical domains
  - Comparison with analytic solutions

- Single and multiple processor calculations yield identical results

- Future directions

- More complex geometry
- Magnetostatic problem
  - Must deal with gauge condition
- Reconstruction of force-free fields from boundary data
- Resistive MHD

## Implementation

- Standard Fortran 90

- Object-oriented features

<http://www.cs.rpi.edu/~szymanski/oof90.html>

- Parallelization

- Runs on serial and parallel machines

- MPI

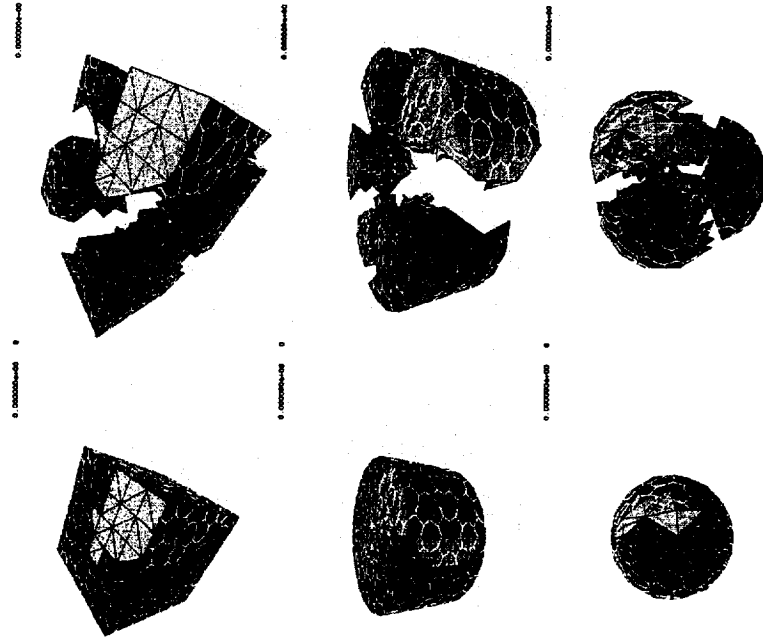
<http://www.mpi-forum.org>

- Grid generation with LaGrIT (LANL)
- <http://www.t12.lanl.gov/~lagrit>

## Mesh Partitioning between 5 PEs

### Implementation (cont.)

- Grid decomposition with Metis (U.Minn.)  
<http://www.cs.unm.edu/~metis>
- Matrix inversion with PETSc (ANL)  
<http://www.mcs.anl.gov/petsc>
- Graphics with GMV (LANL)  
<http://www-xdiv.lanl.gov/XCM/gmv/>



## Test Case: Diffusion Equation

The diffusion equation for the vector potential  $\mathbf{A}$ ,

$$\frac{\partial \mathbf{A}}{\partial t} = -\eta \nabla \times \nabla \times \mathbf{A} + \mathbf{S},$$

is numerically implemented as

$$\begin{aligned}\Delta V \left( \frac{1}{\eta} + \omega \Delta t \nabla \times \nabla \times \right) \Delta \mathbf{A} = \\ -\Delta V \Delta t \nabla \times \nabla \times \mathbf{A}^n + \frac{\Delta V \Delta t}{\eta} \mathbf{S}.\end{aligned}$$

$\Delta V$  Element of volume

$\Delta t$  Time step

$\eta$  Resistivity

$\omega$  Factor between 1/2 and 1

$\mathbf{S}$  Source term

The operator on  $\Delta \mathbf{A}$  is self-adjoint in our formulation.

## Numerical vs. Analytical Solution of Diffusion Equation: Box

- A solution of the diffusion equation in a box domain:

$$A_z = \exp(-\nu t) \sin\left(\frac{n_x \pi x}{L_x}\right) \sin\left(\frac{n_y \pi y}{L_y}\right)$$

- If

$$\begin{aligned}L_x &= L_y & n_x &= n_y = 1, \\ \eta &= 0.01\end{aligned}$$

Then

$$\nu_{\text{Analytical}} = 0.197.$$

- Using 125 nodes, 383 cells in a  $1 \times 1 \times 1$  cubic domain and  $\Delta t = 0.01$ ,

$$\nu_{\text{Numerical}} = 0.182.$$

## Numerical vs. Analytical Solution of Diffusion Equation: Sphere

- A solution of the diffusion equation in a sphere:

$$A_z = \exp(-\nu t) \left( \frac{\sin(kr)}{(kr)^2} - \frac{\cos(kr)}{(kr)} \right) \sin \theta$$

- A solution of the diffusion equation in a cylinder:

$$A_z = \exp(-\nu t) J_0(kr)$$

- If

$$\begin{aligned} k &= 4.493 \\ \eta &= 0.01 \end{aligned}$$

Then

$$\nu_{\text{Analytical}} = 0.202$$

$$\nu_{\text{Analytical}} = 0.231$$

- Using 513 nodes, 2519 cells in a spherical domain of  $R = 1$  and  $\Delta t = 0.01$ ,

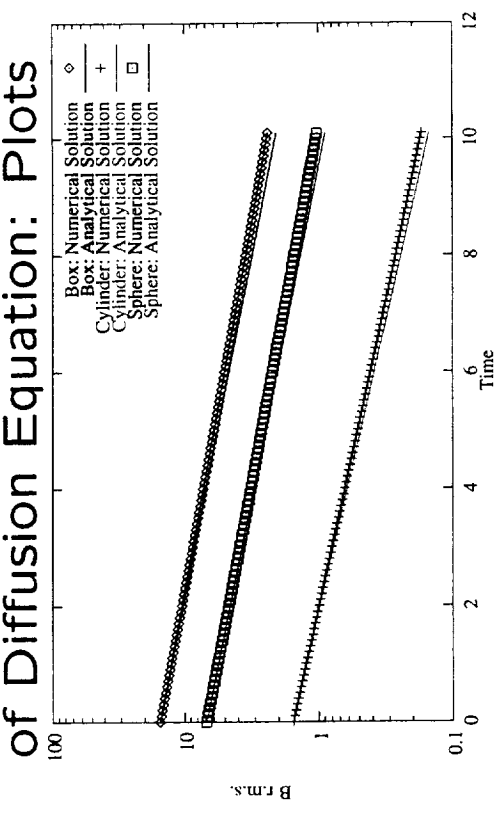
$$\nu_{\text{Numerical}} = 0.188$$

- Using 500 nodes, 1704 cells in a cylindrical domain of  $h = R = 1$  and  $\Delta t = 0.01$ ,

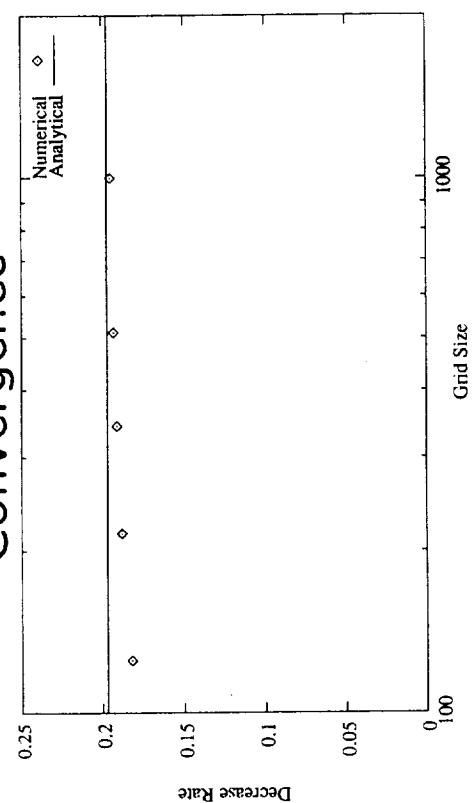
$$\nu_{\text{Numerical}} = 0.218$$

## Numerical vs. Analytical Solution of Diffusion Equation: Cylinder

# Numerical vs. Analytical Solution of Diffusion Equation:



# Numerical vs. Analytical Solution of Diffusion Equation: Convergence



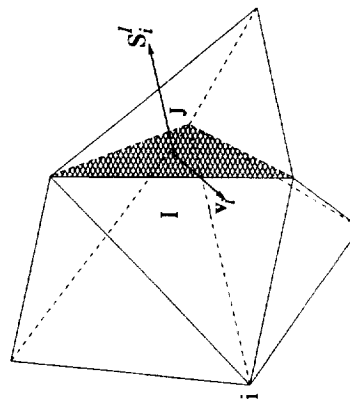
## Density Advection

- Advection equation:

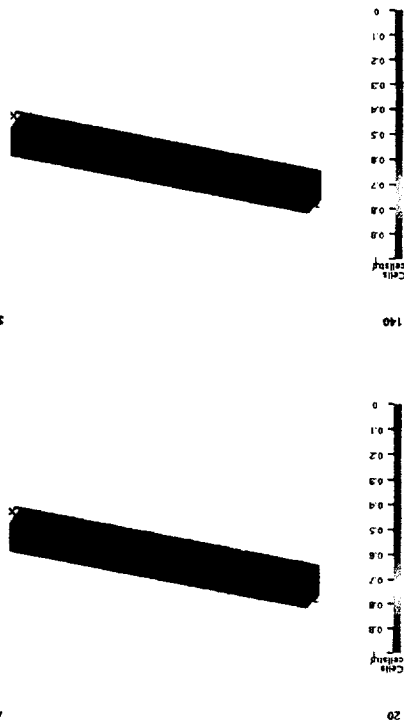
$$\frac{\partial \rho}{\partial t} = -\nabla \cdot \rho \mathbf{v}.$$

- Finite volume formulation with upwinding:

$$\begin{aligned}\frac{\Delta \rho^I}{\Delta t} &= -\frac{1}{V^I} \sum_i S_i^I \cdot \bar{\mathbf{v}}_i \rho^{U(i)}, \\ \rho^{U(i)} &= \begin{cases} \rho^I & \text{if } S_i^I \cdot \bar{\mathbf{v}}_i \geq 0 \\ \rho^J & \text{if } S_i^I \cdot \bar{\mathbf{v}}_i < 0 \end{cases}\end{aligned}$$



## MHD - DENSITY ADVECTION



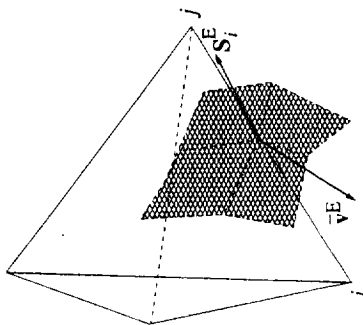
## Momentum Advection

- Advection equation:

$$\frac{\partial \mathbf{p}}{\partial t} = -\nabla \cdot \mathbf{p} \mathbf{v}.$$

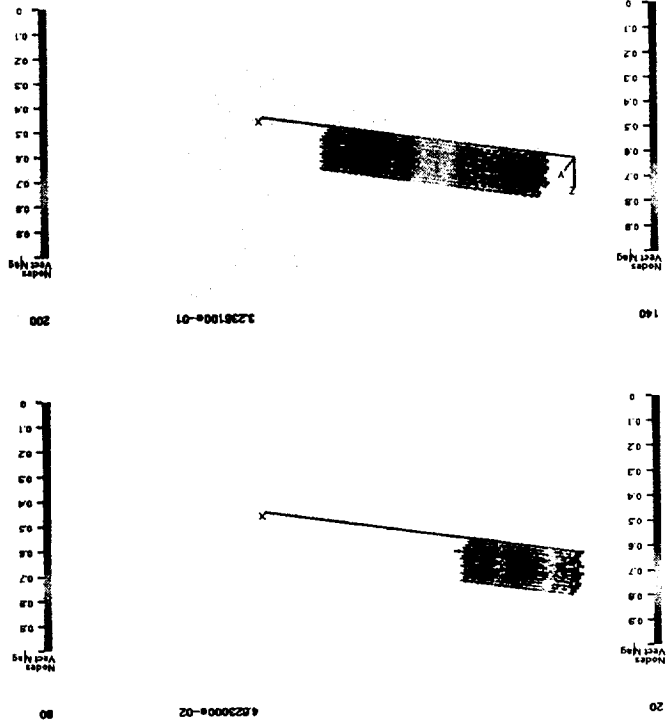
- Finite volume formulation with upwinding:

$$\begin{aligned}\frac{\Delta \mathbf{p}_i}{\Delta t} &= -\frac{1}{V_i} \sum_E \mathbf{S}_i^E \cdot \bar{\mathbf{v}}^E \mathbf{p}_{u(E)}, \\ \mathbf{p}_{u(E)} &= \begin{cases} \mathbf{p}_i & \text{if } \mathbf{S}_i^E \cdot \bar{\mathbf{v}}^E \geq 0 \\ \mathbf{p}_j & \text{if } \mathbf{S}_i^E \cdot \bar{\mathbf{v}}^E < 0 \end{cases}\end{aligned}$$



## MHD - MOMENTUM ADVECTION

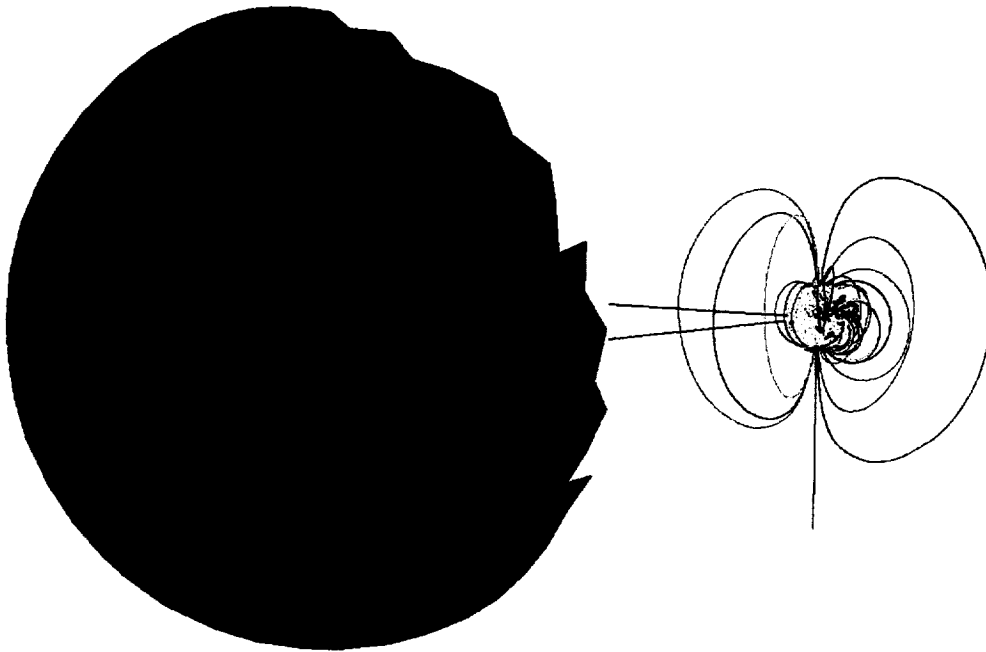
4623000-01  
14592004-01  
4623000-02  
14592004-02  
3236100-01  
4623000-01

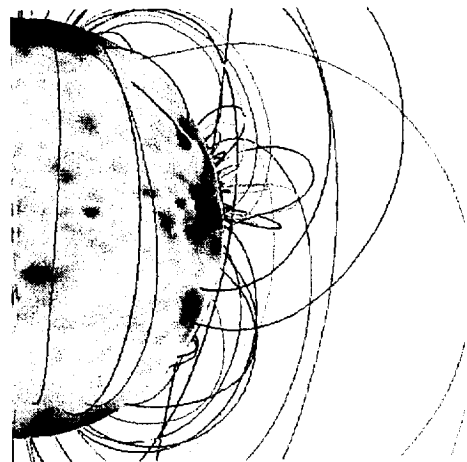


## Potential Models

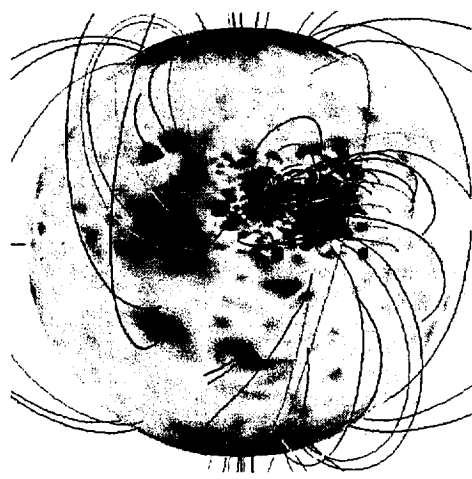
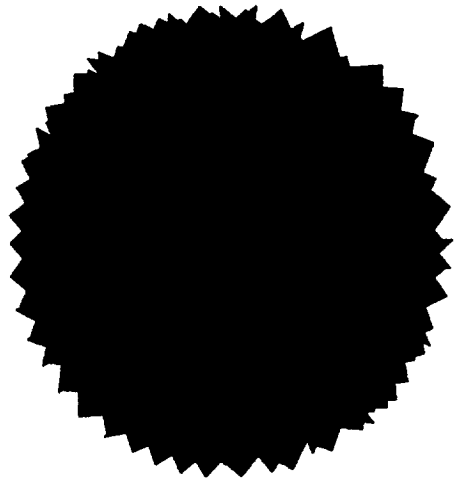
- Active region during Whole Sun Month (August-September 1996).
- Active regions AR8102 and AR8100 (November 1997).
- We use synoptic magnetograms from Kitt Peak National Observatory.
- The grid extends from 1 to  $10 R_{\odot}$ .
- The meshes consist of 42001 (32881) vertices and 242705 (189237) tetrahedra.
- The resolution varies from 8 degrees (outside the active regions) to 1 degree (inside).

## High Resolution and Large Scale Model of the Corona (I)



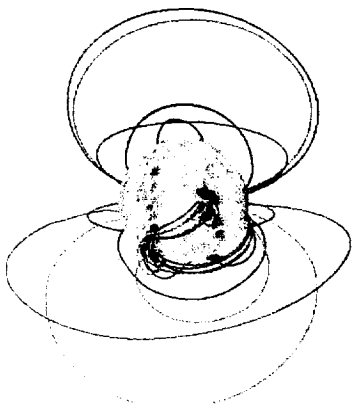


High Resolution and Large Scale Model of the Corona (III)

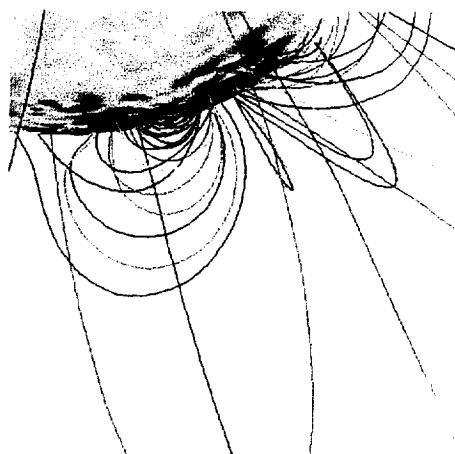
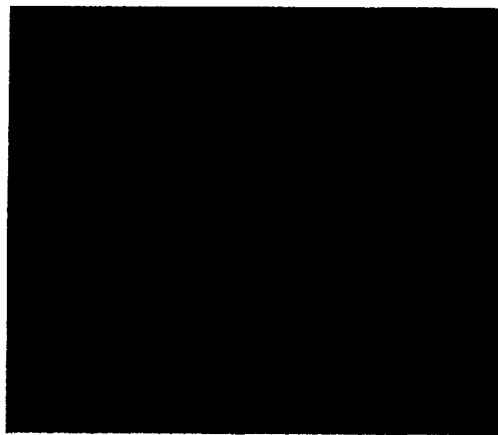


High Resolution and Large Scale Model of the Corona (II)

Magnetogram Data and Field Lines



Tetrahedral Mesh

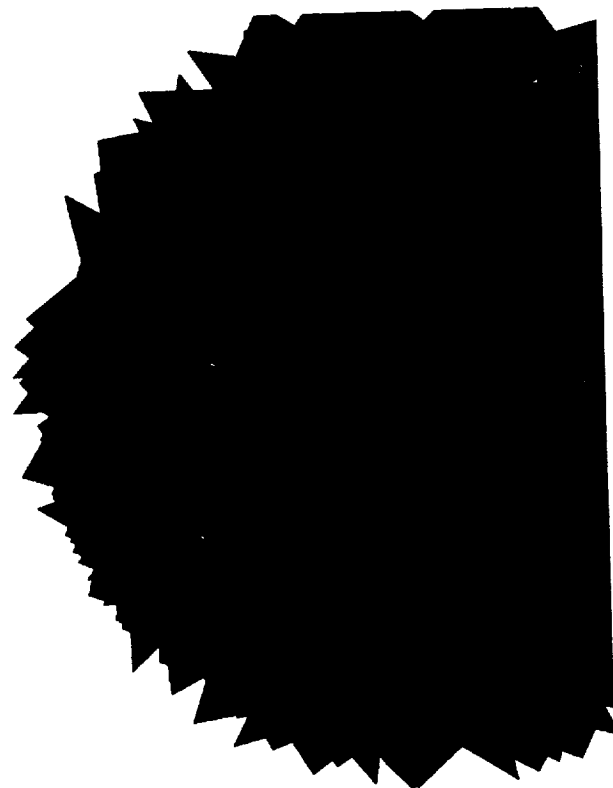


High Resolution and Large Scale Model of the Corona (IV)

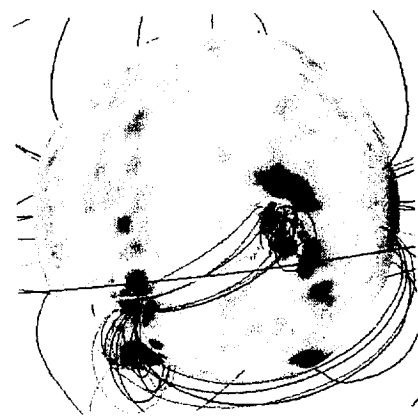
**Magnetogram Data and Field Lines**



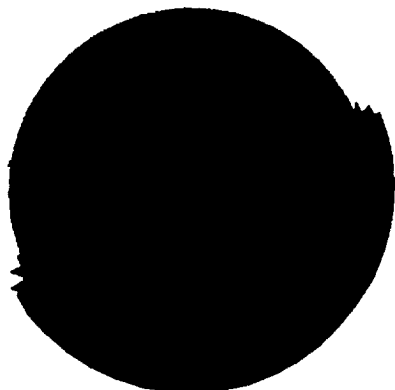
**Tetrahedral Mesh**



**Magnetogram Data and Field Lines**



**Tetrahedral Mesh**



# REPORT DOCUMENTATION PAGE

*Form Approved  
OMB No. 0704-0188*

Public reporting burden for this collection of information is estimated to average 1 hour per response, including the time for reviewing instructions, searching existing data sources, gathering and maintaining the data needed, and completing and reviewing the collection of information. Send comments regarding this burden estimate or any other aspect of this collection of information, including suggestions for reducing this burden, to Washington Headquarters Services, Directorate for Information Operations and Reports, 1215 Jefferson Davis Highway, Suite 1204, Arlington, VA 22202-4302, and to the Office of Management and Budget, Paperwork Reduction Project (0704-0188), Washington, DC 20506.

1. AGENCY USE ONLY (Leave Blank)			2. REPORT DATE August 15, 2001	3. REPORT TYPE AND DATES COVERED 2nd Year 4th Quarter Progress Report 5/16/00-8/15/01
4. TITLE AND SUBTITLE  The Structure and Dynamics of the Solar Corona and Inner Heliosphere: 2nd Year 4th Quarter Progress Report			5. FUNDING NUMBERS NAS5-99188	
6. AUTHORS Zoran Mikic				
7. PERFORMING ORGANIZATION NAME(S) AND ADDRESS(ES)  Science Applications International Corporation 10260 Campus Point Drive San Diego, CA 92121-1578			8. PERFORMAING ORGANIZATION REPORT NUMBER SAIC-01/8013:APPAT-280 01-0157-04-2065-000	
9. SPONSORING/MONITORING AGENCY NAME(S) AND ADDRESS(ES)  NASA Headquarters Operation Office Goddard Space Flight Center Greenbelt, MD 20771			10. SPONSORING/MONITORING AGENCY REPORT NUMBER	
11. SUPPLEMENTARY NOTES				
12a. DISTRIBUTION/AVAILABILITY STATEMENT			12b. DISTRIBUTION CODE	
13. ABSTRACT ( <i>Maximum 200 words</i> )  This report details progress during the fourth quarter of the second year of the Sun-Earth Connections Theory Program contract, "The Structure and Dynamics of the Solar Corona and Inner Heliosphere."				
14. SUBJECT TERMS  Solar Corona, Coronal Magnetic Field, Heliosphere, Magnetohydrodynamics			15. NUMBER OF PAGES 64	
			16. PRICE CODE	
17. SECURITY CLASSIFICATION OF REPORT  UNCLASSIFIED	18. SECURITY CLASSIFICATION OF THIS PAGE  UNCLASSIFIED	19. SECURITY CLASSIFICATION OF ABSTRACT  UNCLASSIFIED	20. LIMITATION OF ABSTRACT  UL	